Top

Left side

TEST

Right side

Bottom

Datos 3

Luis A. Orozco
lorozco@umd.edu
www.jqi.umd.edu

Lección 8 en el Departamento de Física
Universidad de Concepción
Marzo 2024

https://www.physics.umd.edu/rgroups/amo/orozco/results/2024/Results24.htm

Ejemplo de reporte de errores

PHYSICAL REVIEW A **70**, 042504 (2004)

Lifetimes of the 9*s* and 8*p* levels of atomic francium

S. Aubin,* E. Gomez, L. A. Orozco,† and G. D. Sprouse
Department of Physics and Astronomy, State University of New York, Stony Brook, New York 11794-3800, USA
(Received 10 May 2004; published 20 October 2004)

We use time-correlated single-photon counting techniques on a sample of ^{210}Fr atoms confined and cooled in a magneto-optical trap to measure the lifetimes of the $9S_{1/2}$, $8P_{3/2}$, and $8P_{1/2}$ excited levels. We populate the $9S_{1/2}$ level by two-photon resonant excitation through the $7P_{1/2}$ level. The direct measurement of the $9S_{1/2}$ decay through the $7P_{3/2}$ level at 851 nm gives a lifetime of 107.53±0.90 ns. We observe the decay of the $9S_{1/2}$ level through the $8P_{3/2}$ level at 423 nm and the $8P_{1/2}$ level at 433 nm down to the $7S_{1/2}$ ground level, and indirectly determine the lifetimes of these to be 83.5±1.5 ns and 149.3±3.5 ns, respectively.

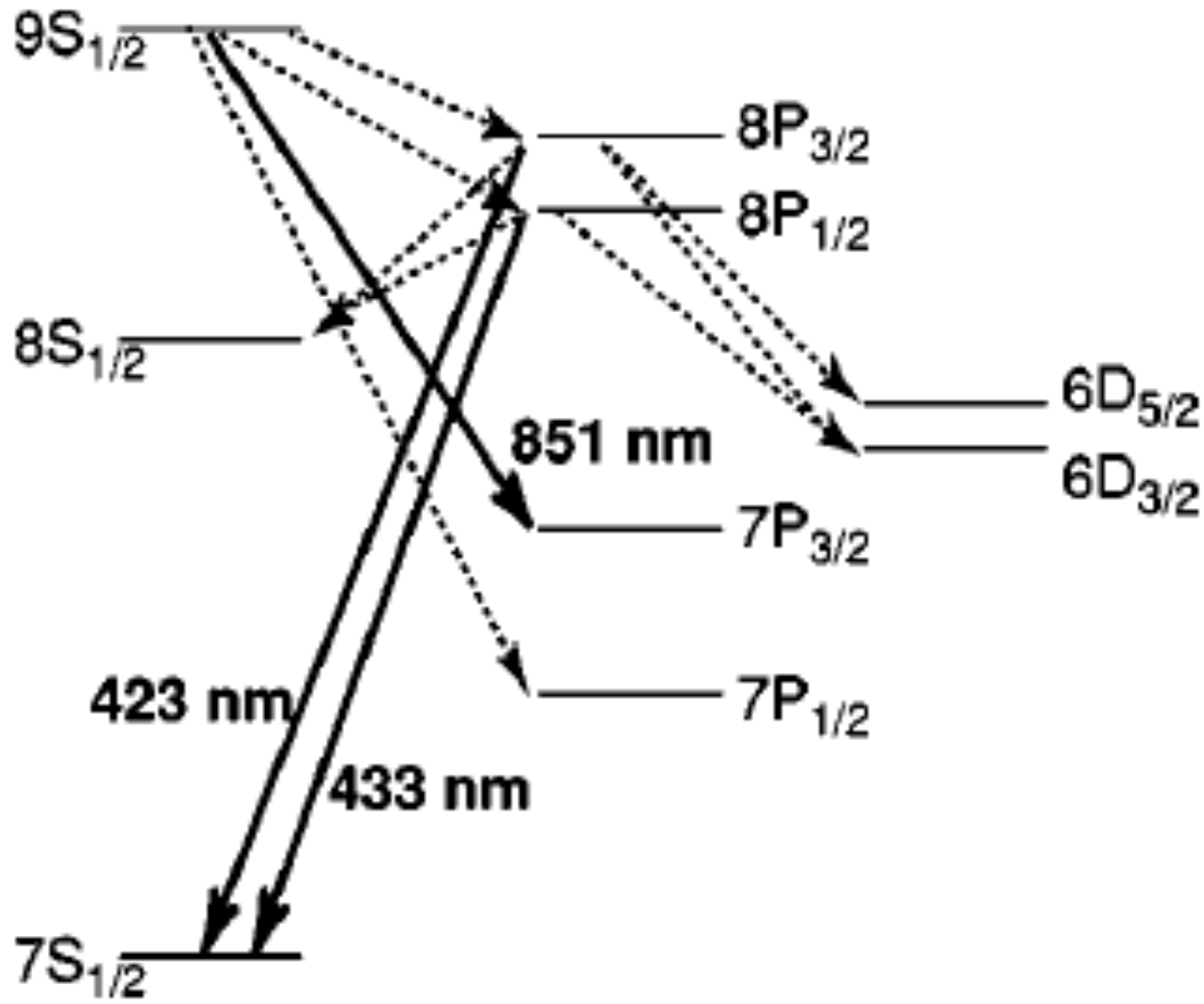
9S1/2
8P3/2
8P1/2
8S1/2
6D5/2
6D3/2
851 nm
7P3/2
7P1/2
423 nm
433 nm
7S1/2

(a) *TAC and MCA nonlinearity*. We calibrate the timing of the $8P_{3/2}$ pulse detection apparatus in the same manner as the for $9S_{1/2}$ measurement. While the technique is the same, the apparatus is physically distinct, and consequently shows some difference in performance. We measure the linear time calibration of the TAC and MCA with an uncertainty of ±0.02%. The time scale has a nonlinearity, which adds an uncertainty of ±0.13% to the lifetime of the fitted data. We find that the height scale of the TAC and MCA taken together varies by roughly 1% over 1000 channels. This nonuniformity in the height scale influences the fitted lifetime by less than 0.13%.

(b) *Pulse pileup correction*. We keep this correction small by maintaining count rates of about one event every 50 cycles. The correction to the data provided by Eq. (2) affects the fitted lifetime of our data by less than 0.07%.

(c) *Truncation error*. We find that varying the start and end points of the data set does not lead to statistically significant changes in the fitted lifetime.

(d) *Quantum beats*. We populate the energy eigenstates of the $8p$ levels incoherently from the decay of the $9s$ level through the spontaneous emission of a photon. The loss of coherence between energy eigenstates during spontaneous emission eliminates the possibility of quantum beats in the decay of the $8p$ levels. The error due to variations in the filling rate of the $8P_{3/2}$ level from quantum beats in the decay of the $9s$ level are automatically included in the Bayesian error (see below) due to uncertainty in the $9s$ lifetime.

(e) *Contamination shift*. We find a contamination shift of $\delta\tau_2 = -0.10 \pm 0.04$ ns. The shift is much smaller than the statistical error on τ_2.

(f) *Bayesian error*. Since we do not extract the $9s$ lifetime, τ_1, from fits of the $8p$ data, the uncertainty in τ_1 affects the precision with which τ_2 can be extracted in a fit of the data. This source of uncertainty is Bayesian, since it is conditioned on our knowledge of τ_1. τ_1 and τ_2 are not independent variables. The probability that the $8P_{3/2}$ lifetime is given by τ_2' is

$$P(\tau_2') = \int P(\tau_1', \tau_2') d\tau_1' = \int P(\tau_2'|\tau_1') P(\tau_1') d\tau_1'$$

$$= \frac{1}{\sqrt{2\pi}\sigma_1} \int P(\tau_2'|\tau_1') \exp\left(-\frac{1}{2} \frac{(\tau_1' - \tau_1)^2}{\sigma_1^2} \right) d\tau_1', \tag{13}$$

$$P(\tau_2'|\tau_1') = \frac{1}{\sqrt{2\pi}\sigma_2}\exp\left(-\frac{1}{2}\frac{[\tau_2' - \tau_2(\tau_1')]^2}{\sigma_2^2}\right),$$

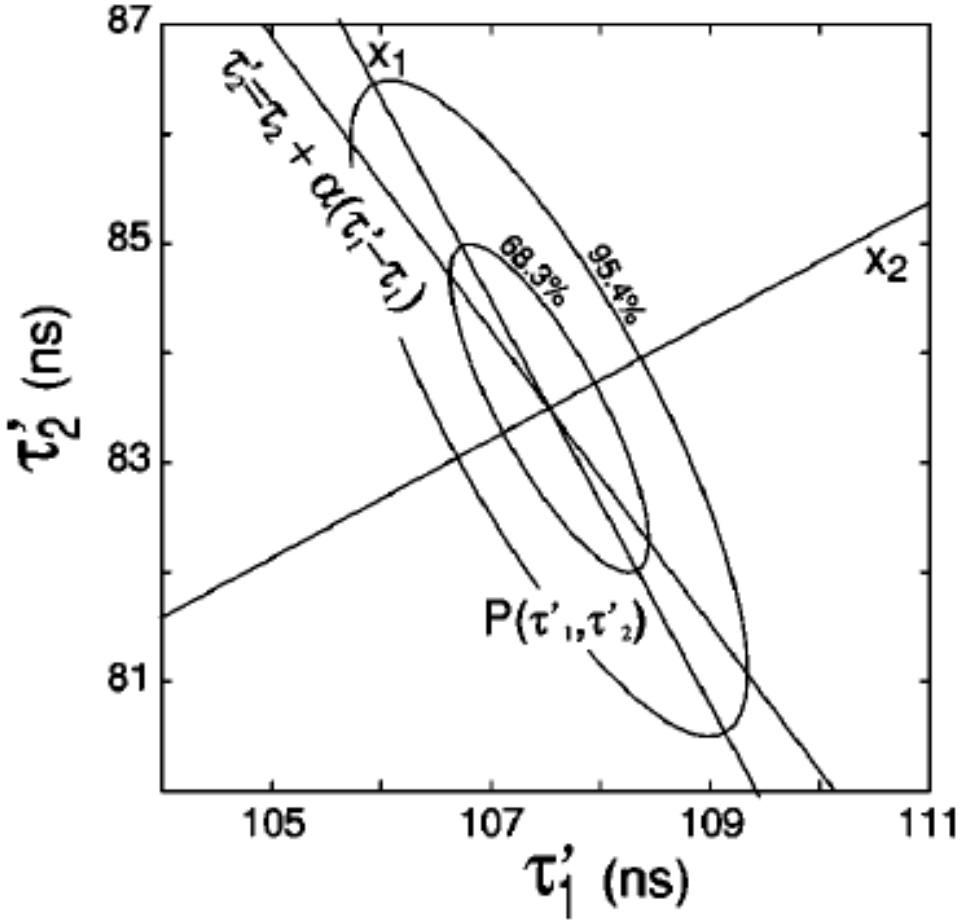

FIG. 11. Probability distribution plot of the $9s$ and $8P_{3/2}$ lifetimes, τ_1 and τ_2. The percentages indicate boundaries of the 68.3% and 95.4% confidence level regions for $P(\tau_1', \tau_2')$. Note that the principal axes of the Gaussian distribution do not coincide with the linear relation for $\tau_2'(\tau_1')$ of Eq. (14).

Un error sistemático

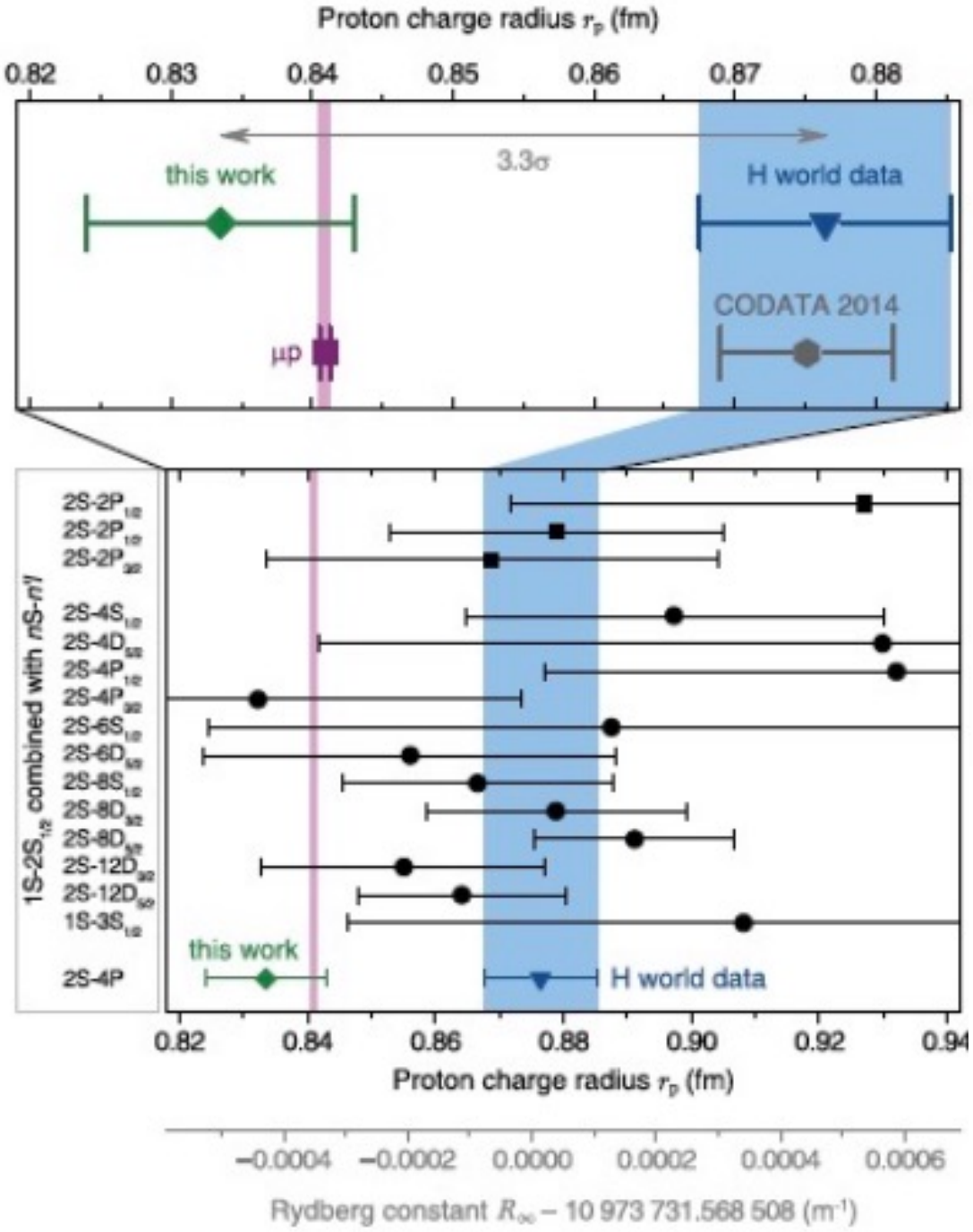

Fig. 1 Rydberg constant R_∞ and proton RMS charge radius r_p. Values of r_p derived from this work (green diamond) and spectroscopy of μp (μp: pink bar and violet square) agree. We find a discrepancy of 3.3 and 3.7 combined standard deviations with respect to the H spectroscopy world data (*12*) (blue bar and blue triangle) and the CODATA 2014 global adjustment of fundamental constants (*3*) (gray hexagon), respectively. The H world data consist of 15 individual measurements (black circles, optical measurements; black squares, microwave measurements). In addition to H data, the CODATA adjustment includes deuterium data (nine measurements) and elastic electron scattering data. An almost identical plot arises when showing R_∞ instead of r_p because of the strong correlation of these two parameters. This is indicated by the R_∞ axis shown at the bottom.

El problema del fondo

¿Como afecta el fondo (background) la incertidumbre?

Si la señal S está sobre un fondo F y el ruido es (Poissoniano)

$$\frac{S}{N} = \frac{S}{\sqrt{S+F}}$$

Mucho cuidado pues el fondo puede dominar completamente la razón señal a ruido.

Además el fondo puede ser afectado por otros sistemáticos.

Pulso y señal

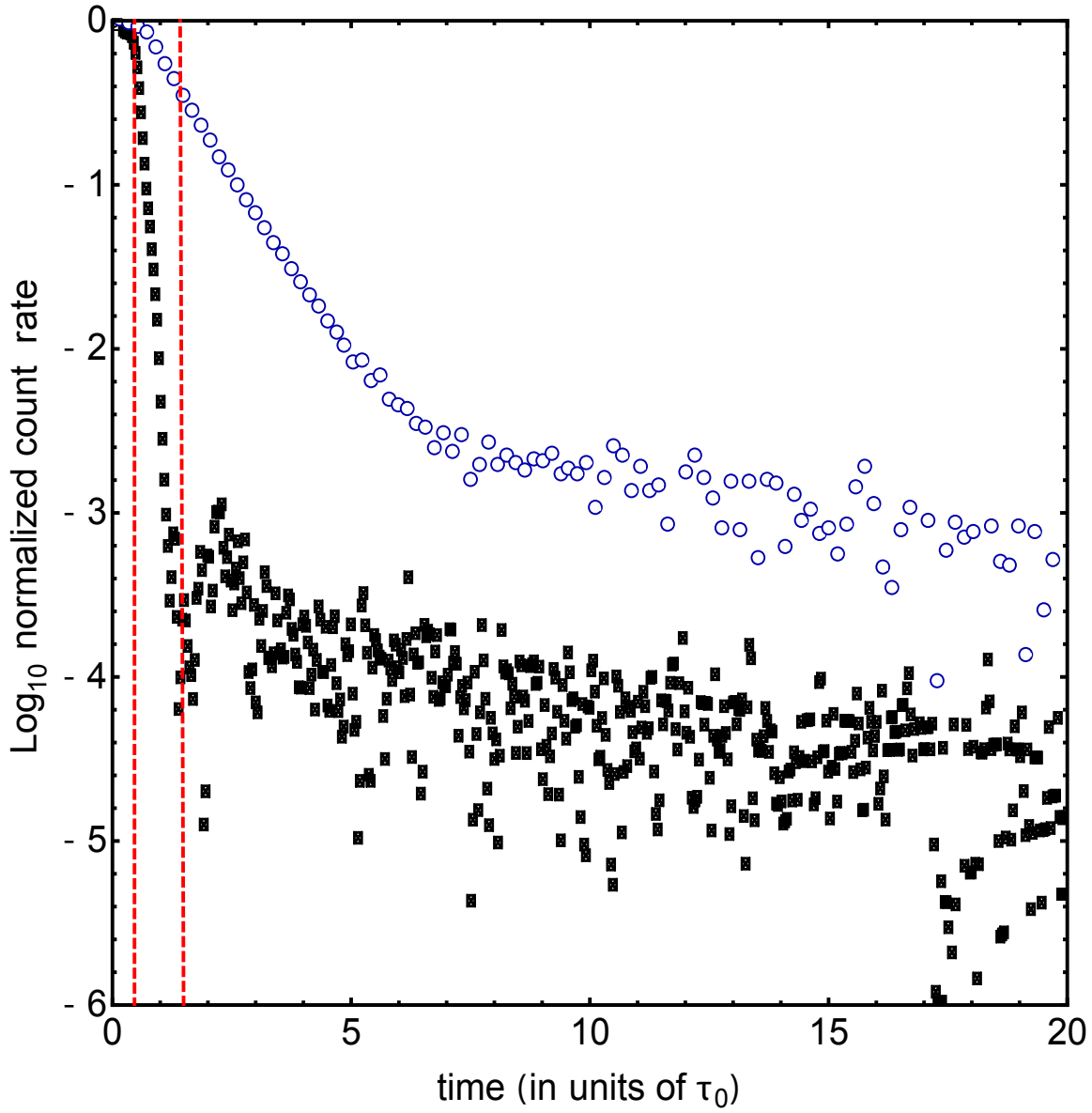

Dos tasas de decaimiento distintas

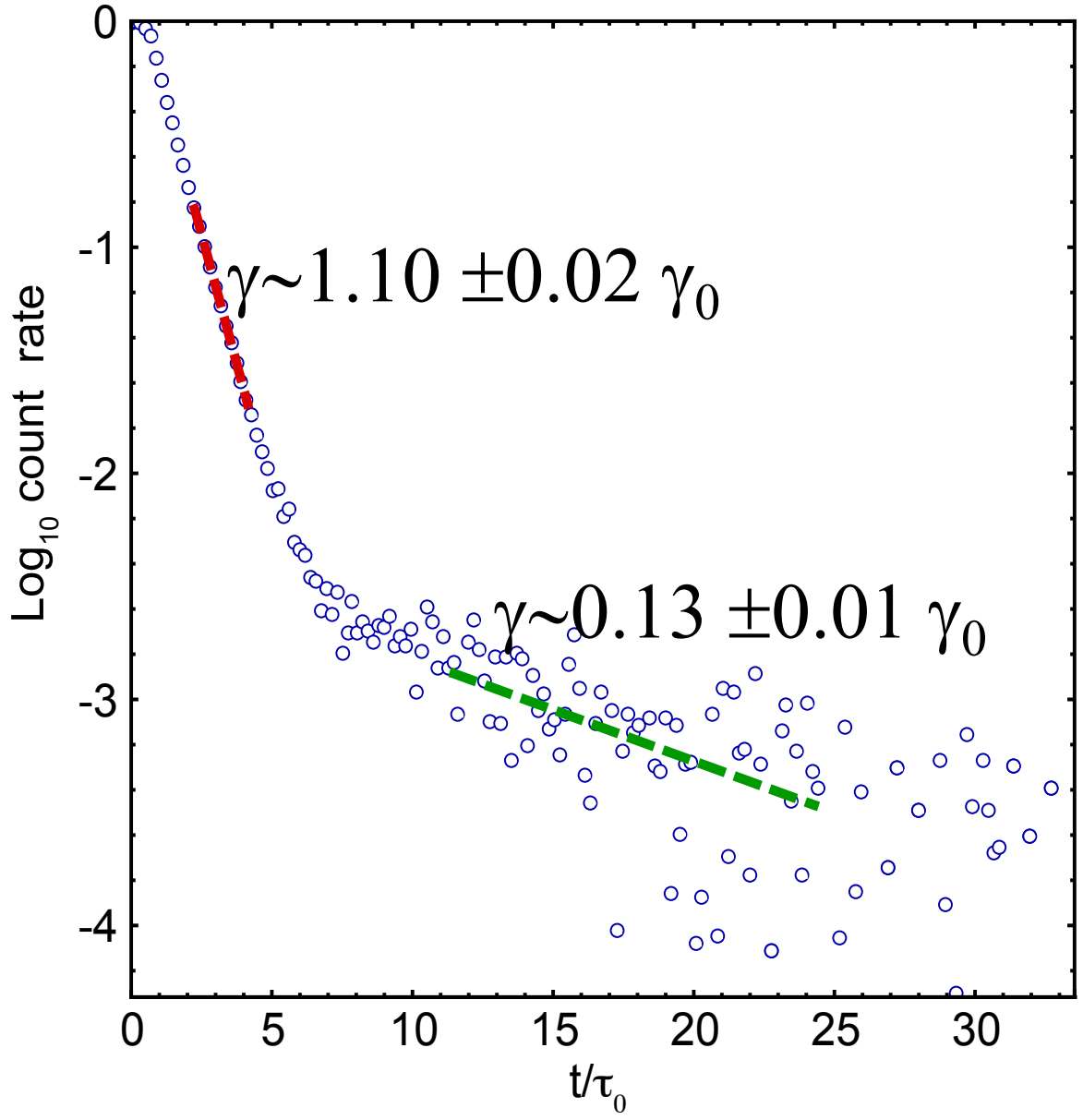

Verde modelo con un solo modo.
pulso ~13 ns

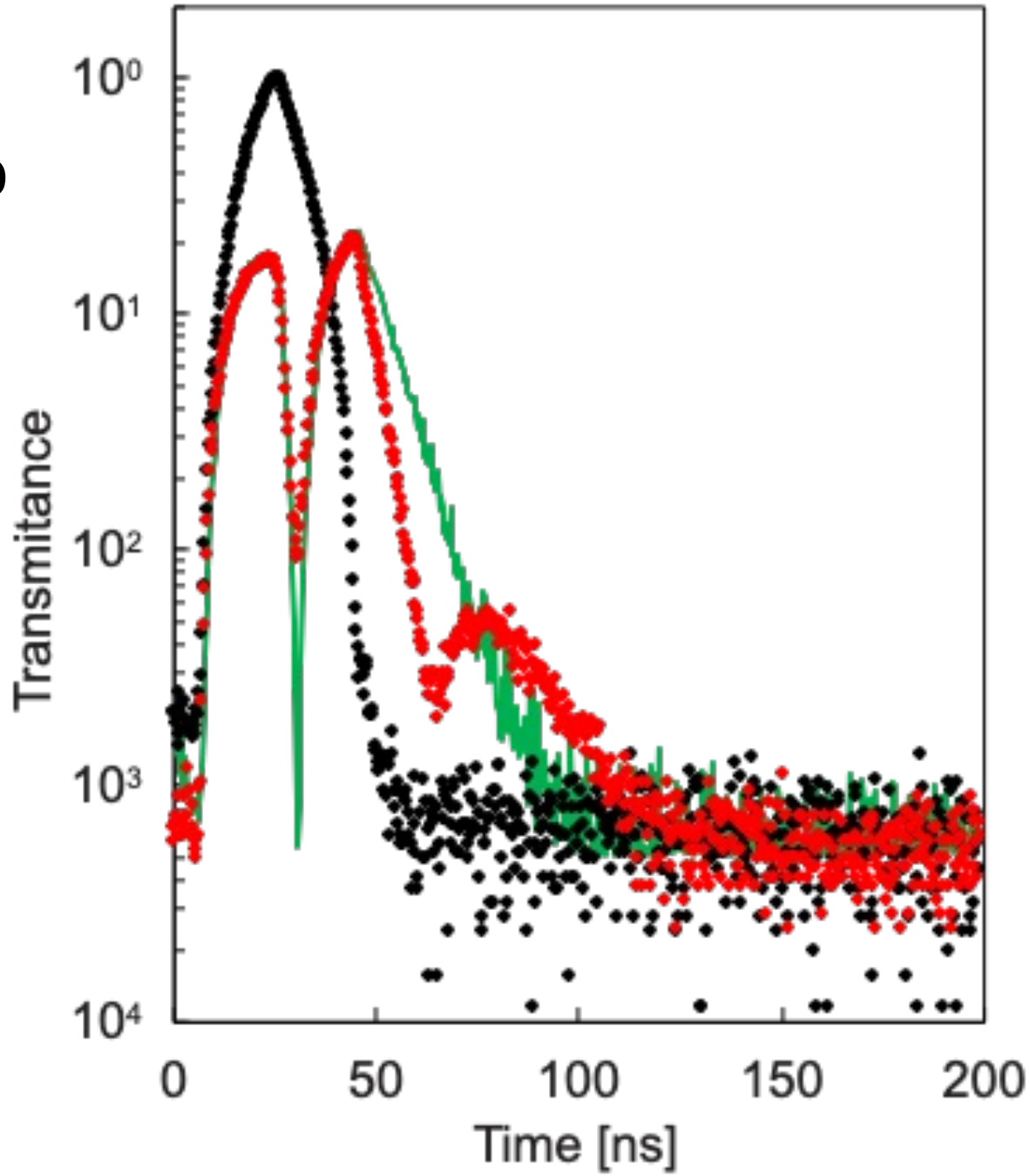

Ruido de disparo

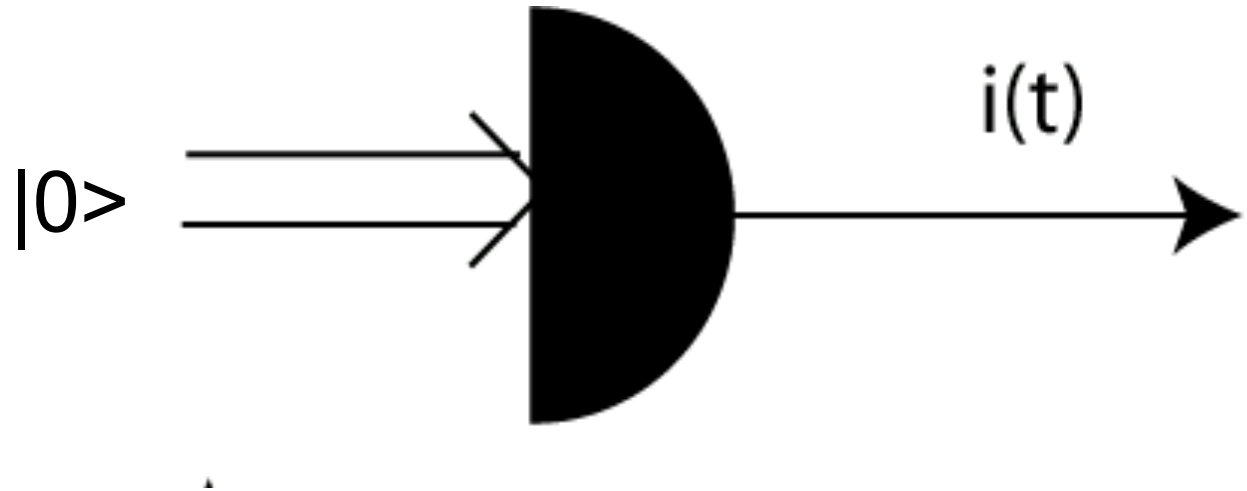

¿Cuánto es la corriente de salida?

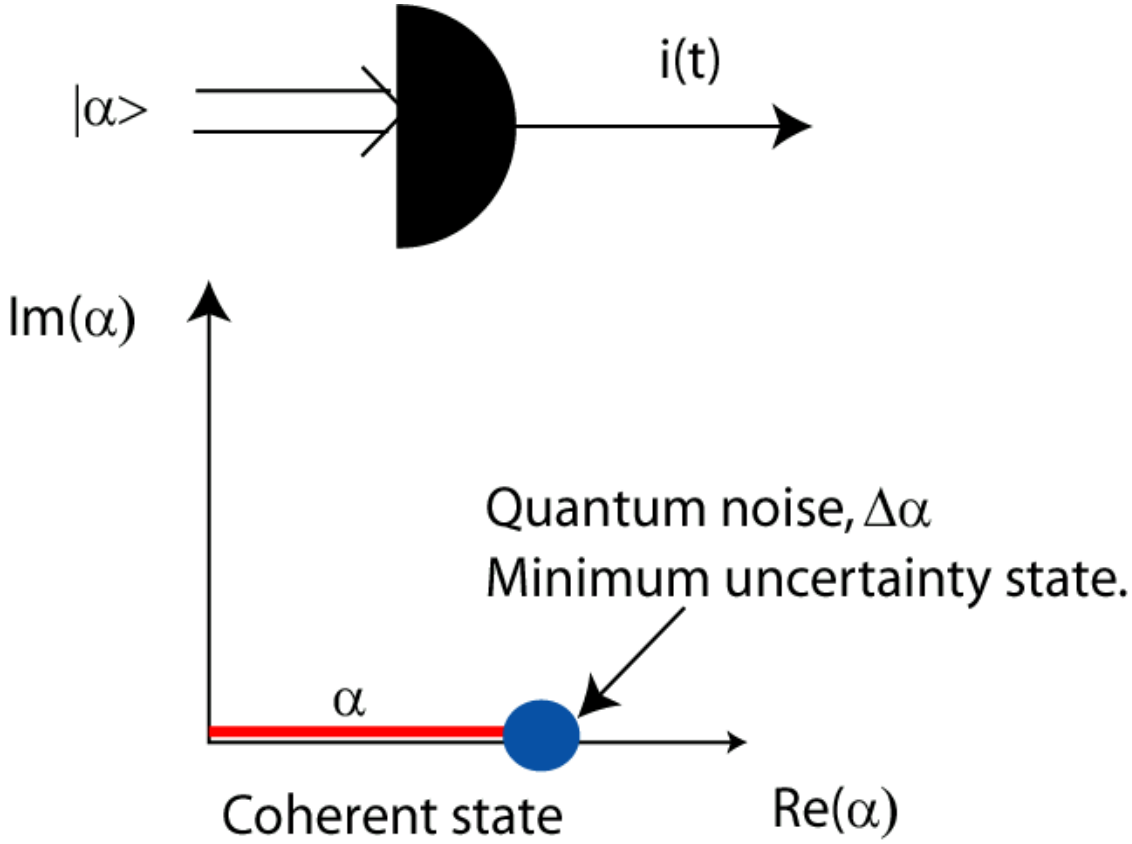

Detector perfecto $i(t) \sim |\alpha + \Delta\alpha|^2$

$$i(t) \sim |\alpha|^2 + 2\ \alpha\,\Delta\alpha + |\Delta\alpha|^2 \quad ; \quad \langle\alpha^*\alpha\rangle = n$$

DC~n Ruido de disparo~$n^{1/2}$ despreciar.

Detección de Luz (ruido de disparo)

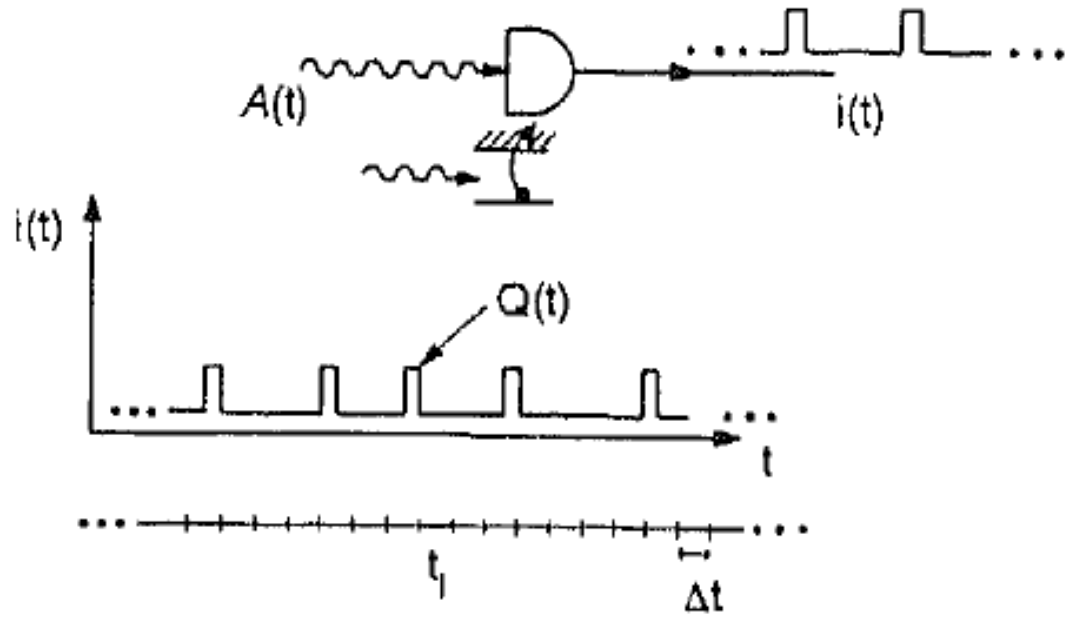

El campo A(t) produce una fotocorriente con carga Q. La ionización sucede en un periodo Δt tal que es lo suficientemente pequeño para solo tener un electrón en cada Δt. p_k es una variable aleatoria.

$$i(t) = \sum_k Q(t - t_k)p_k.$$

H. J. Kimble

$$\langle \Delta i(t) \Delta i(t+\tau) \rangle = Q_0 i_0 [\delta(\tau) + \alpha T \langle : z_0(t), z_0(t+\tau) : \rangle],$$

$$\Phi(\Omega, \theta) = Q_0 i_0 [1 + \alpha T S_s(\Omega, \theta)],$$

$$S_s(\Omega, \theta) = \int d\tau \; \mathrm{e}^{-\mathrm{i}\Omega\tau} \langle : z_0(t), z_0(t+\tau) : \rangle.$$

La densidad espectral de potencia del ruido de disparo cuando S=0:

$$\langle (\Delta i(\Omega,\theta))^2 \rangle = \frac{1}{2\pi}\left[\int_{-\Omega-\Delta\Omega/2}^{-\Omega+\Delta\Omega/2} \Phi(\Omega,\theta)\, d\Omega + \int_{\Omega-\Delta\Omega/2}^{\Omega+\Delta\Omega/2} \Phi(\Omega,\theta)\, d\Omega\right]$$

$$\langle (\Delta i(\Omega))^2 \rangle = 2Q_0 i_0 B.$$

Pero en el caso cuando S≠0

$$\langle(\Delta i(\Omega,\theta))^2\rangle = \frac{1}{2\pi}\left[\int_{-\Omega-\Delta\Omega/2}^{-\Omega+\Delta\Omega/2}\Phi(\Omega,\theta)\,d\Omega + \int_{\Omega-\Delta\Omega/2}^{\Omega+\Delta\Omega/2}\Phi(\Omega,\theta)\,d\Omega\right]$$

$$\langle(\Delta i(\Omega))^2\rangle = 2Q_0 i_0 B[1+\xi S(\Omega,\theta)]$$

Tomando en cuenta la propagación, la detección α, la eficiencia de batido η, y la eficiencia de escape de la cavidad ρ, la transmisión del espejo T_0

$$\xi \equiv \alpha\eta^2 T_0\rho$$

Promedio del ruido de disparo;
S/R~100

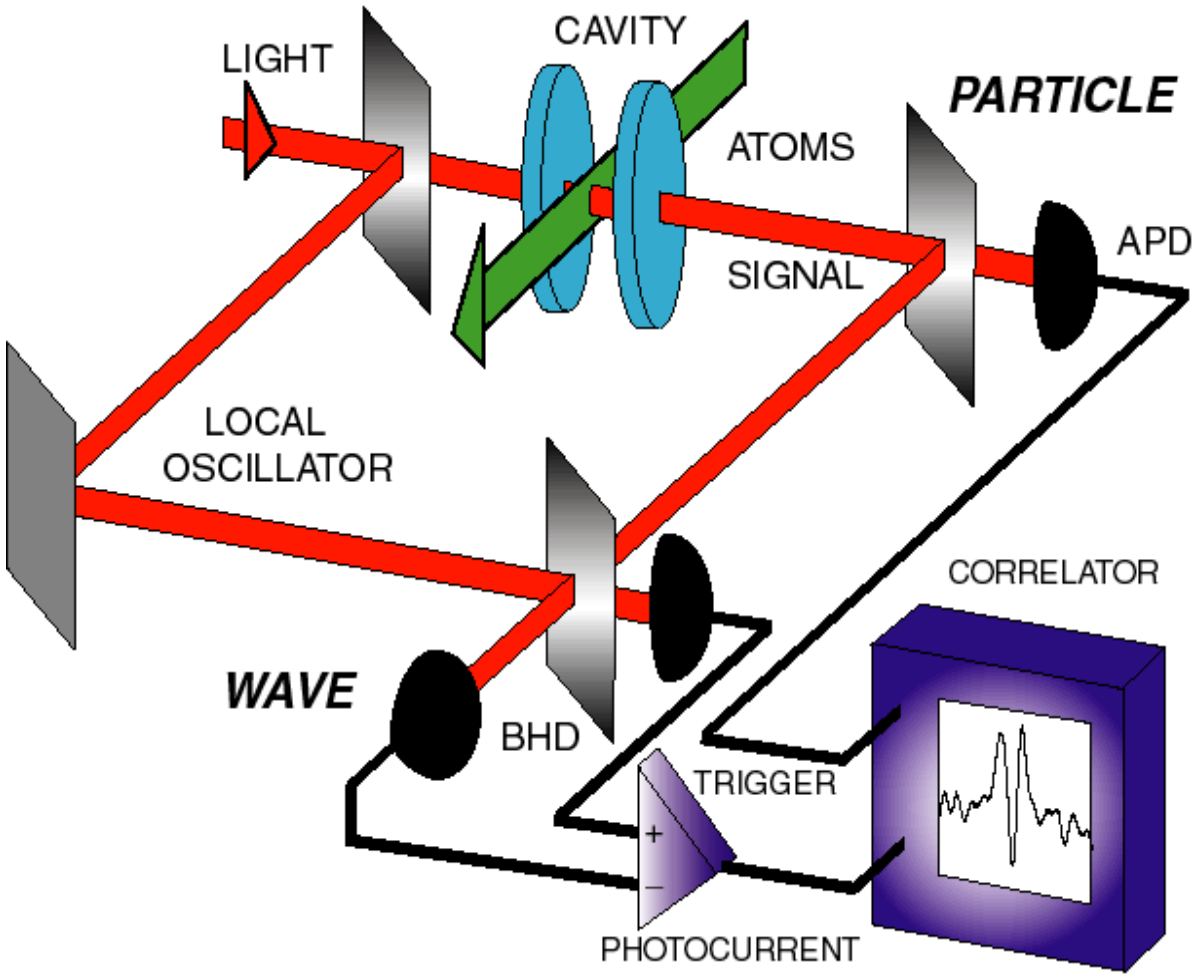

Solo se promedia la fotocorriente si se detecta una fluctuación (fotón)

Fotocorriente condicional sin átomos en la cavidad.

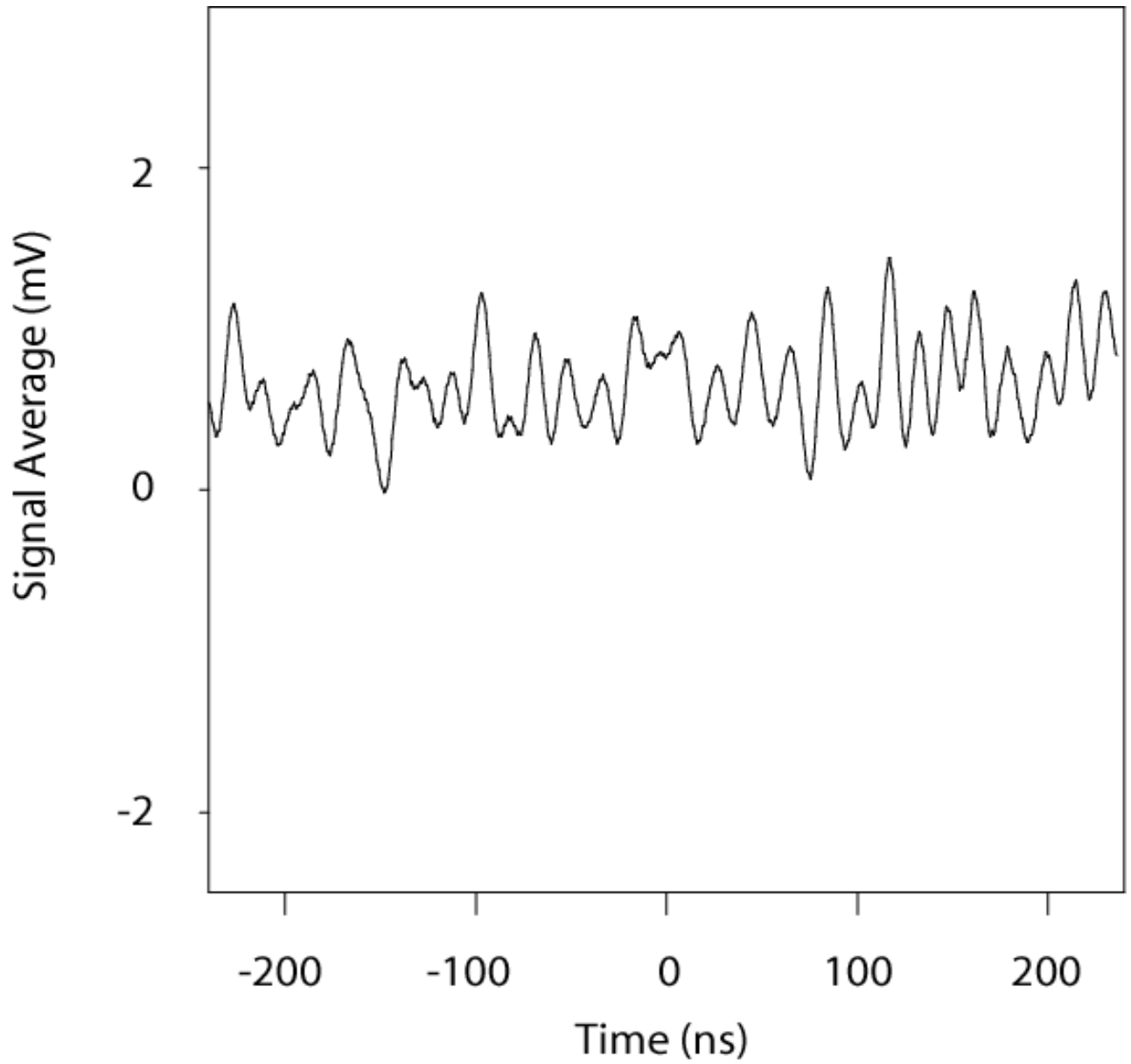

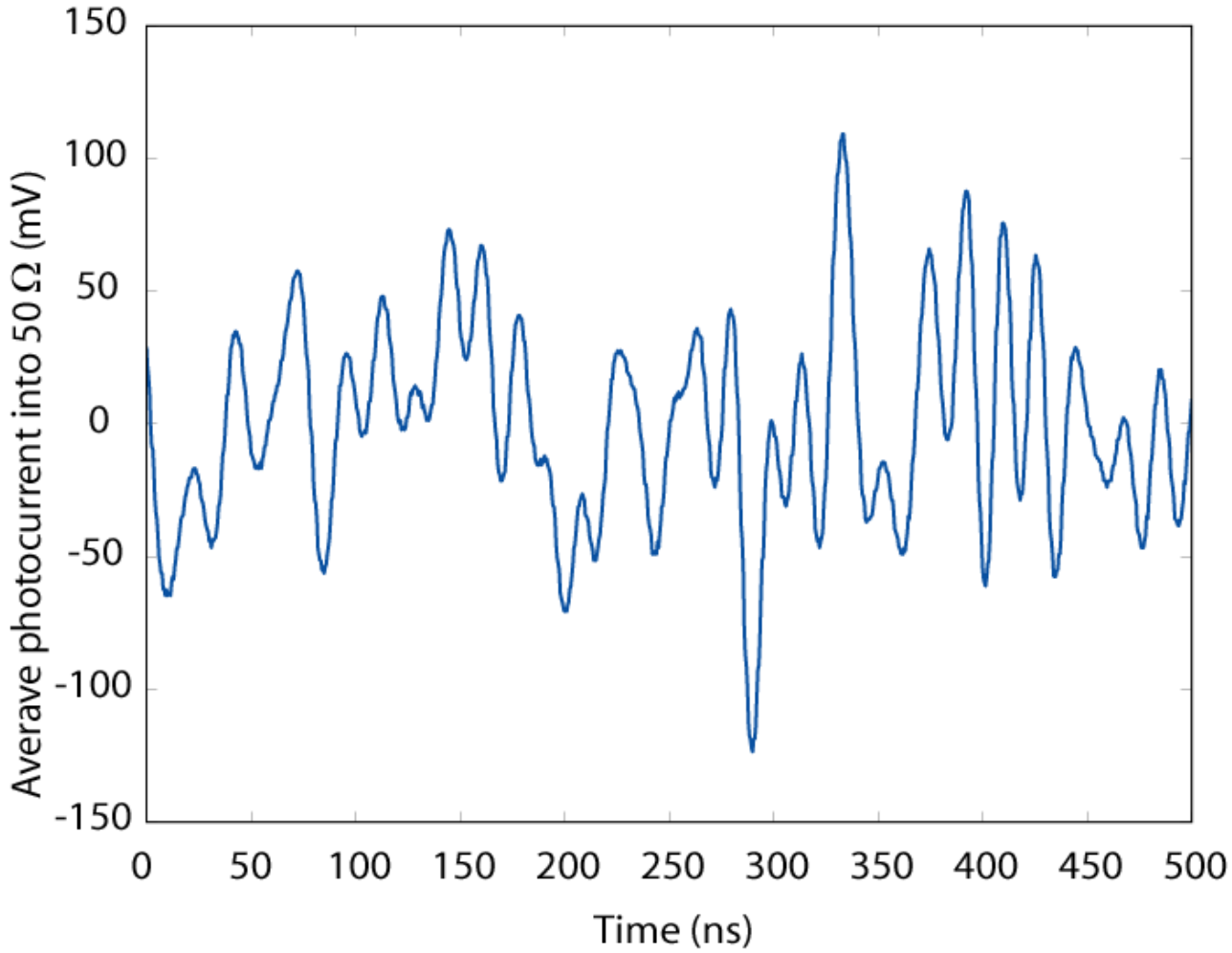

Después de 1 promedio, pp~200 mV

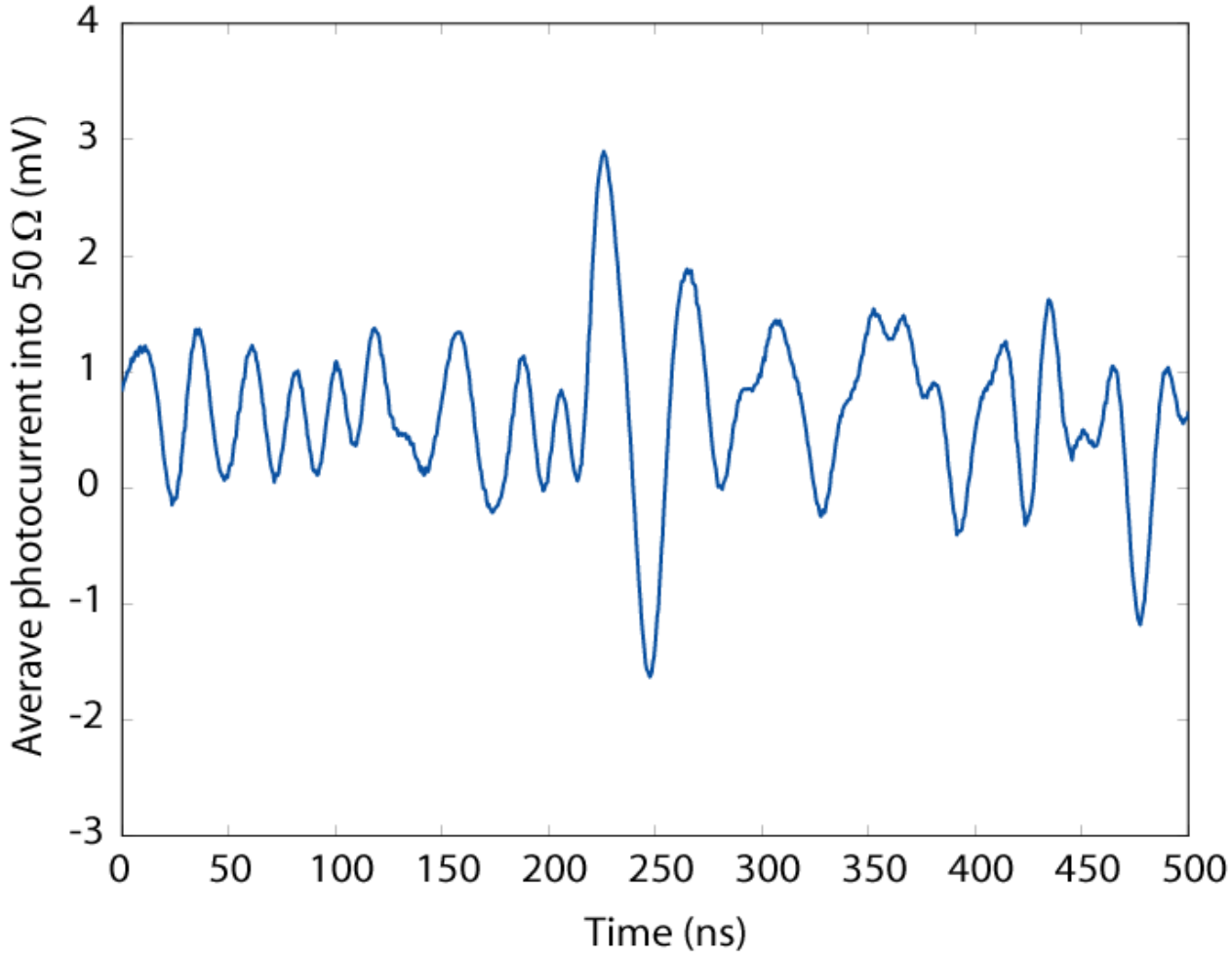

Después de 6.000 promedios

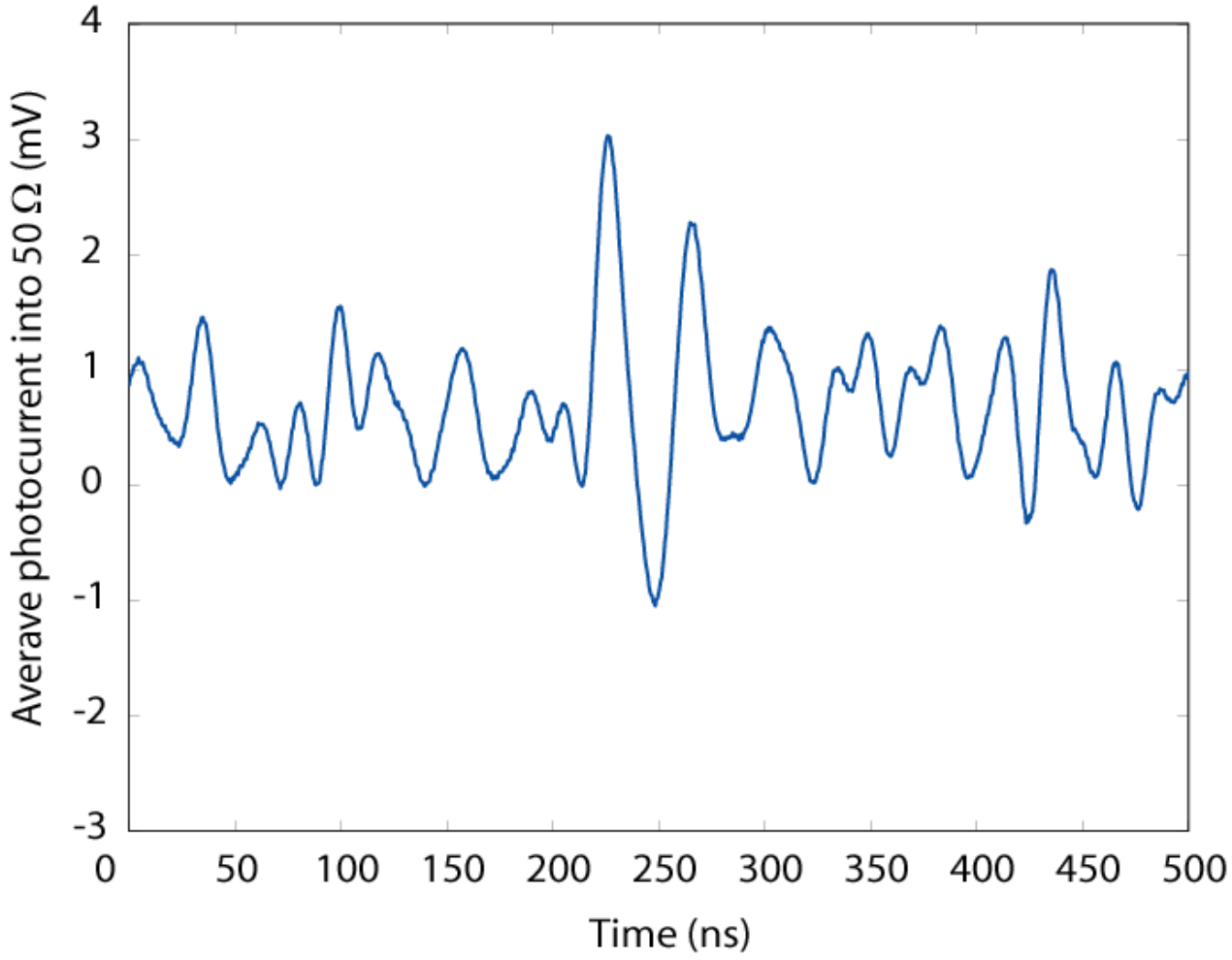

Después de 10.000 promedios

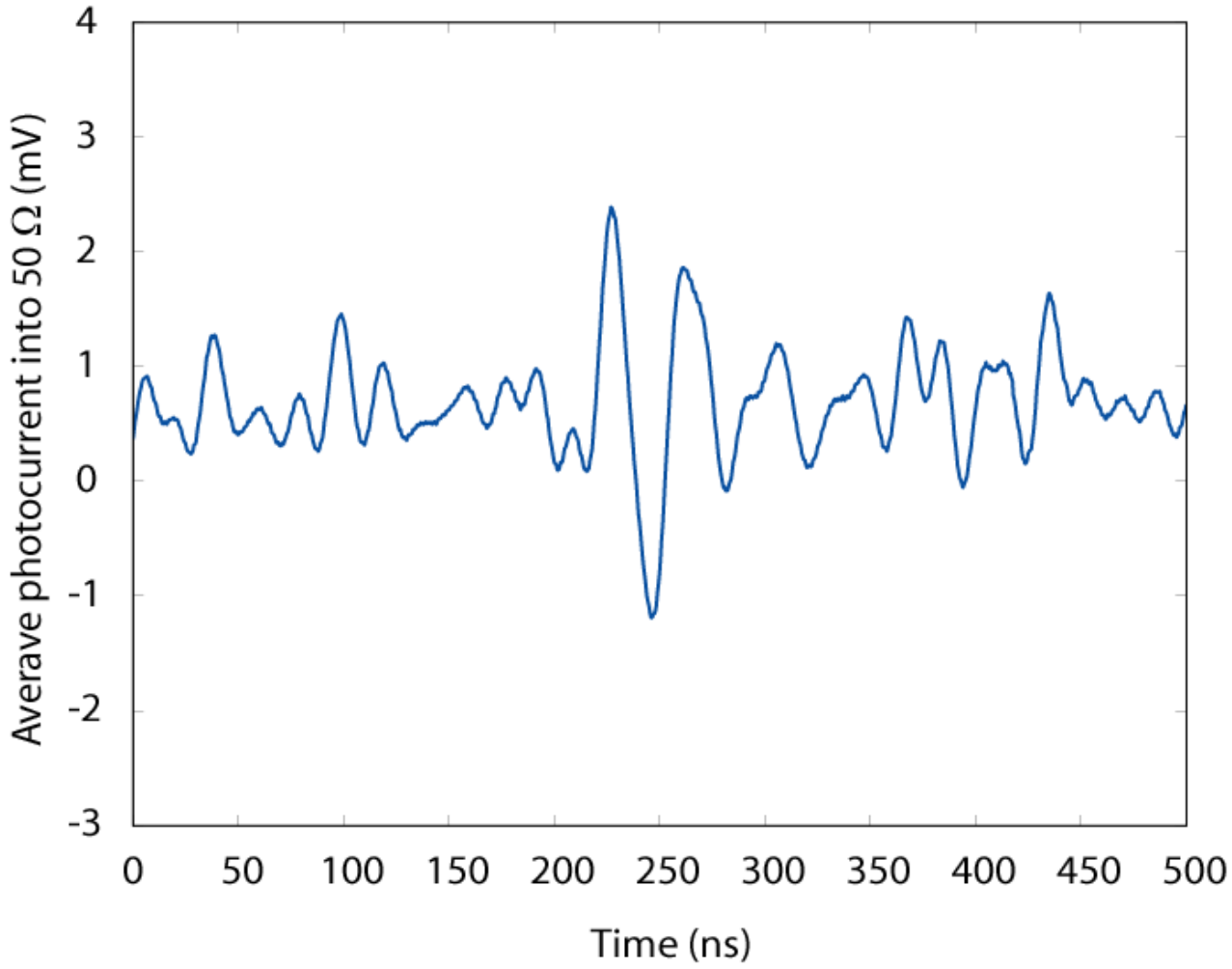

Después de 30.000 promedios

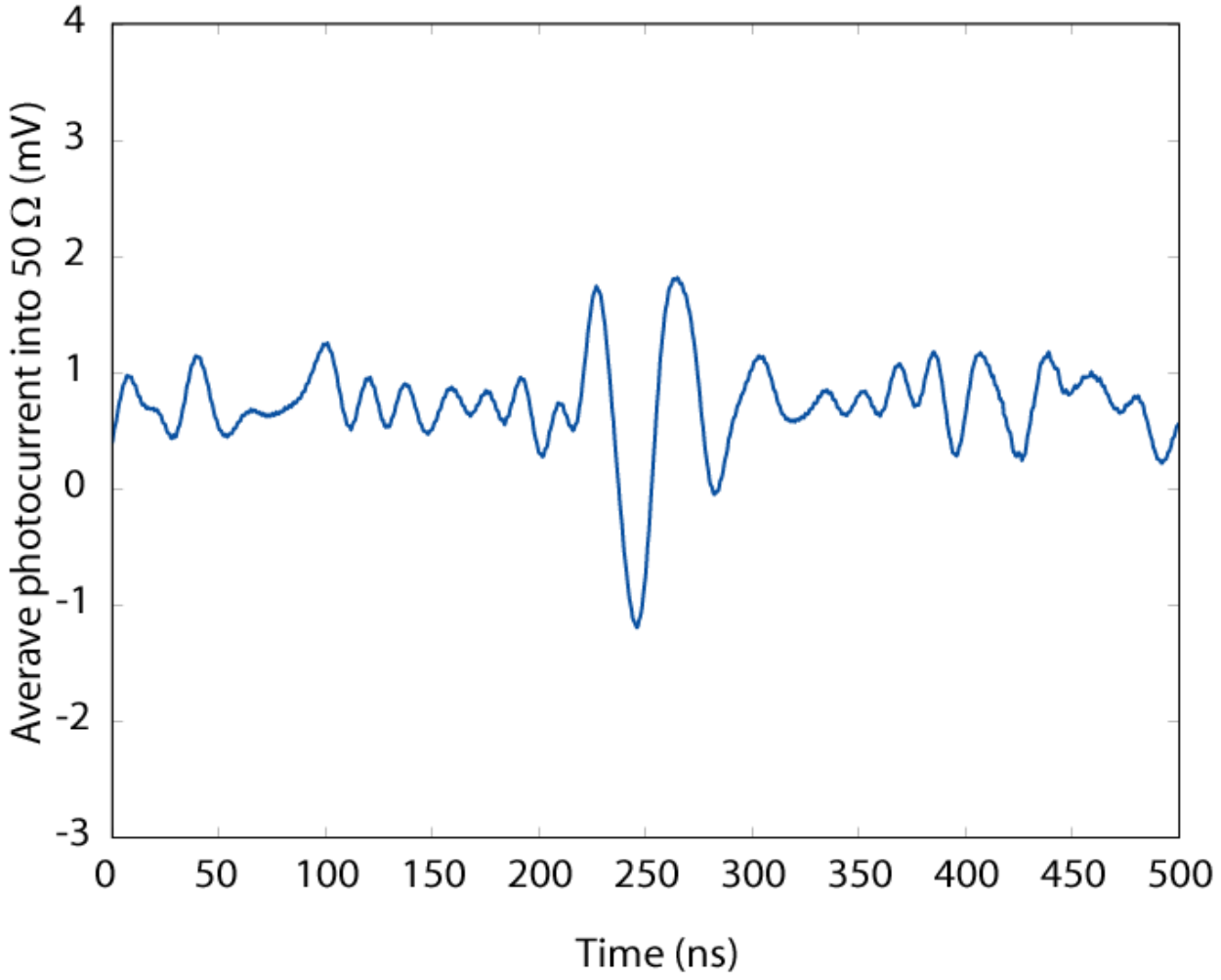

Después de 65,000 promedios, ruido pp ~ 1mV

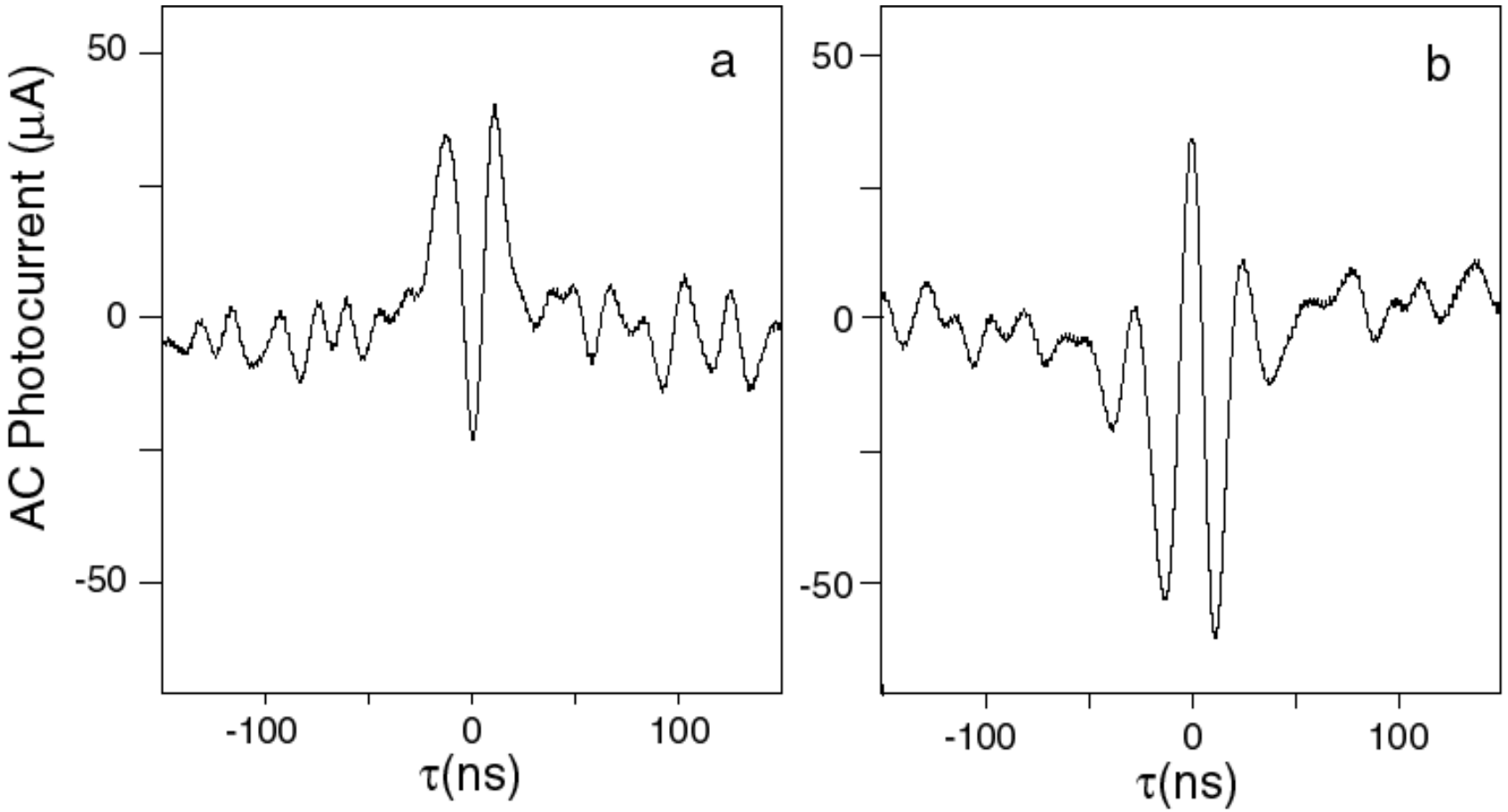

Cambio la fase del Mach-Zehnder por 146º

Squeezing

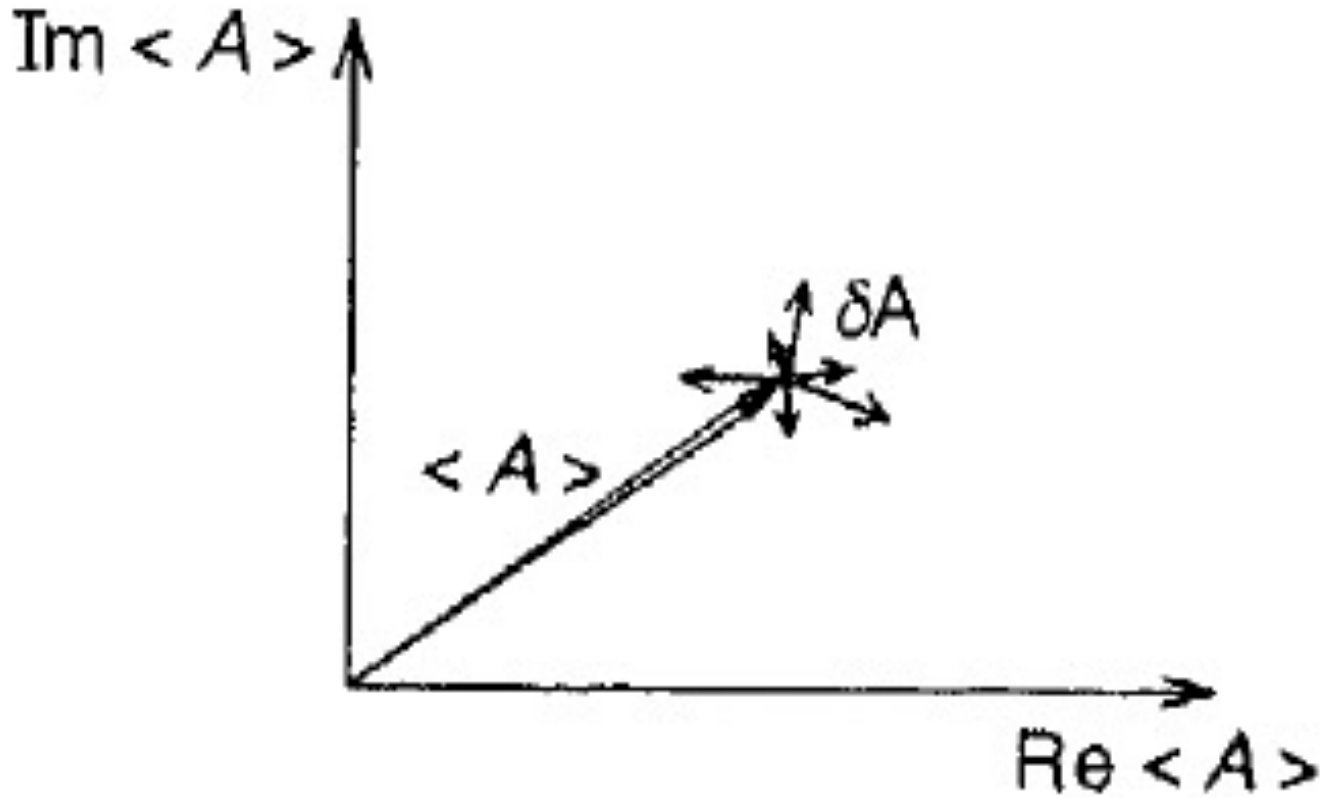
Im < A >
δA
< A >
Re < A >

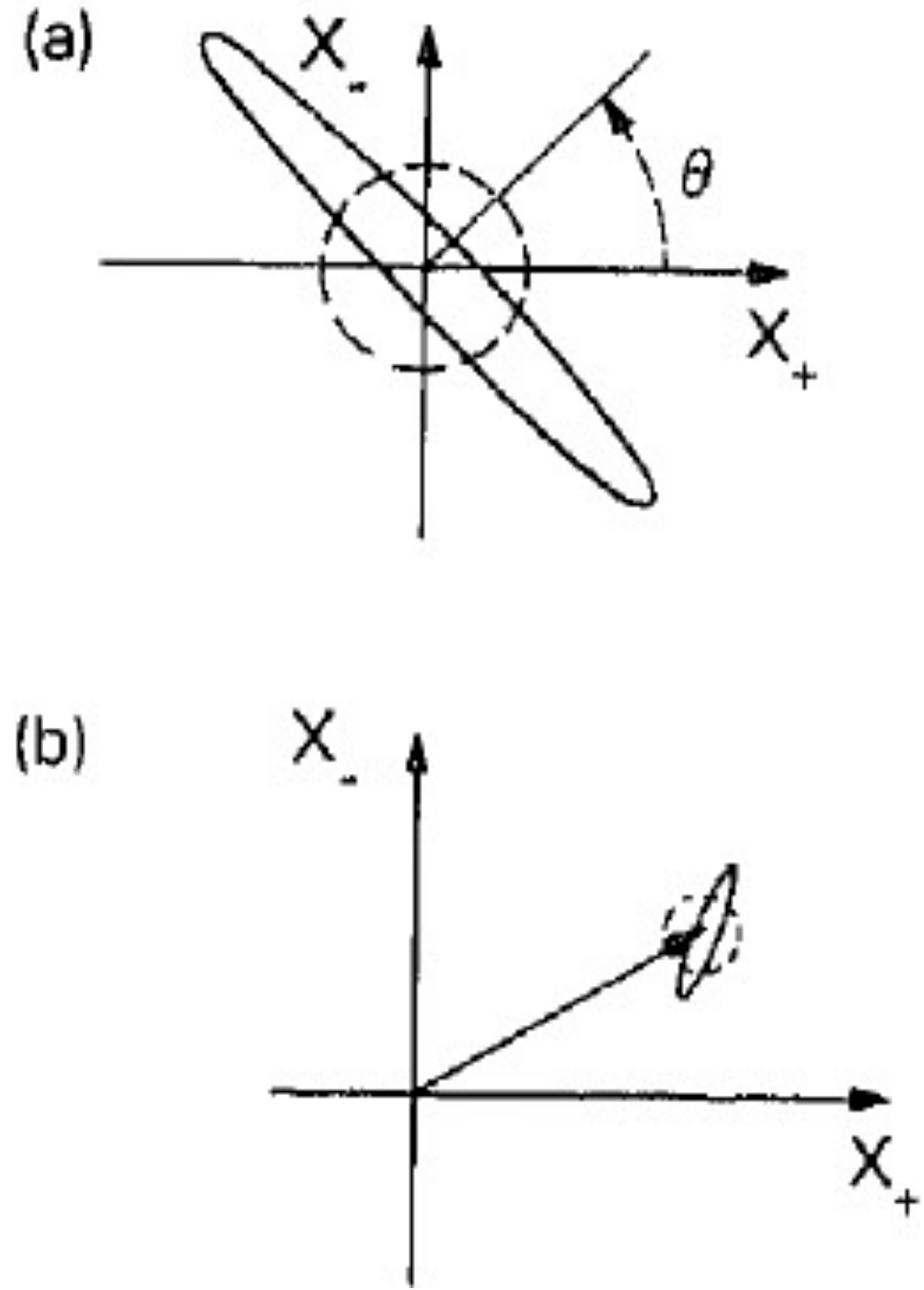
(a)
X-
θ
X+
(b)
X-
X+

$$W(x_+, x_-) = \frac{1}{2\pi\sigma_+\sigma_-} \exp\left[-\tfrac{1}{2}(x_+^2/\sigma_+^2 + x_-^2/\sigma_-^2)\right],$$

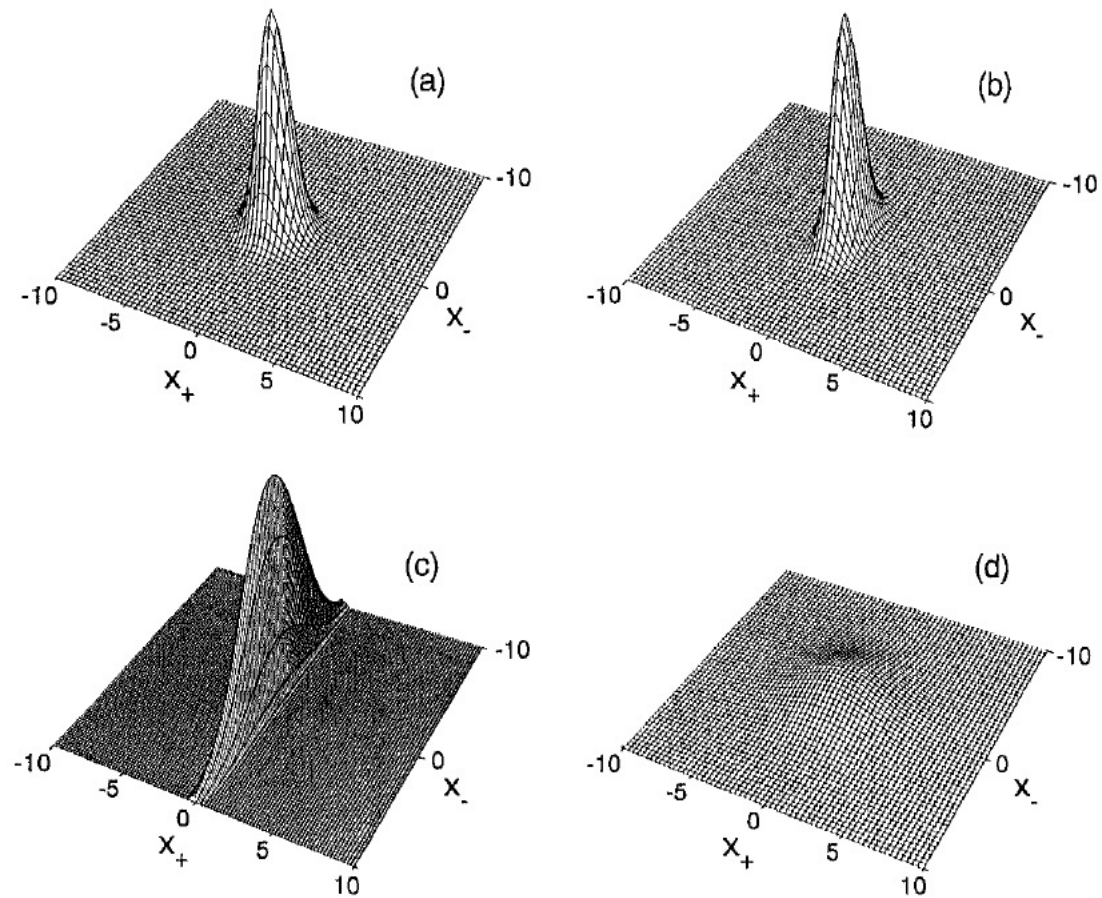

Fig. 12. Wigner distributions for (a) vacuum state, (b) squeezed state with $\sigma_+^2 = 0.5, \sigma_-^2 = 2.0, \langle n\rangle = 0.125$, (c) squeezed state with $\sigma_+^2 = 0.067, \sigma_-^2 = 15.0, \langle n\rangle = 3.3$ and (d) thermal field of mean photon number $\langle n\rangle = 3.3$.

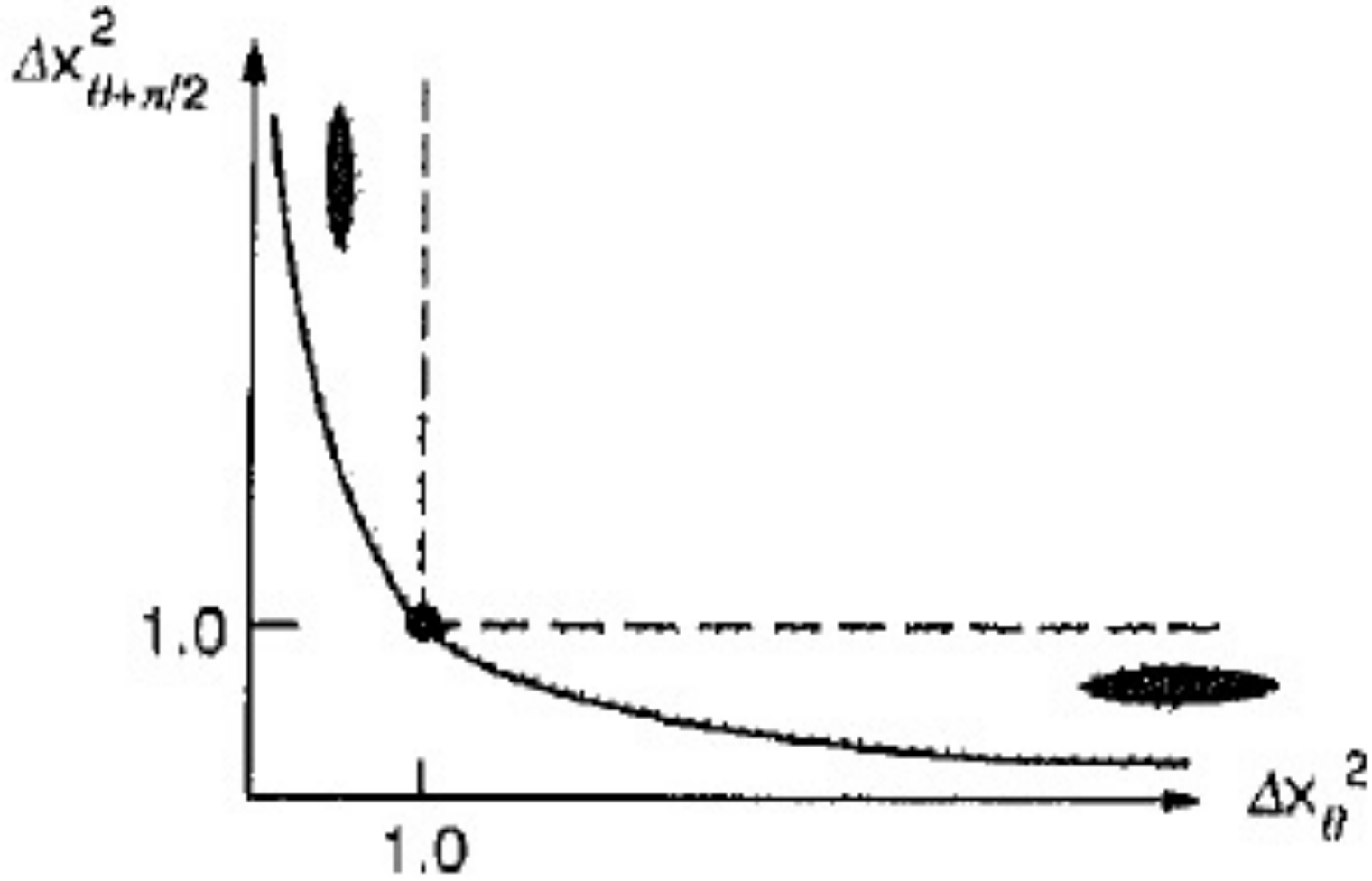
$\Delta x^2_{\theta+\pi/2}$
1.0
1.0
Δx_θ^2

$$\frac{\delta_N + \delta_{S+}}{\sqrt{2}} \qquad \frac{\delta_{s+}^2 + \delta_N^2}{2} > 1$$

$$\delta_{s+}\,\delta_{s-} = 1$$

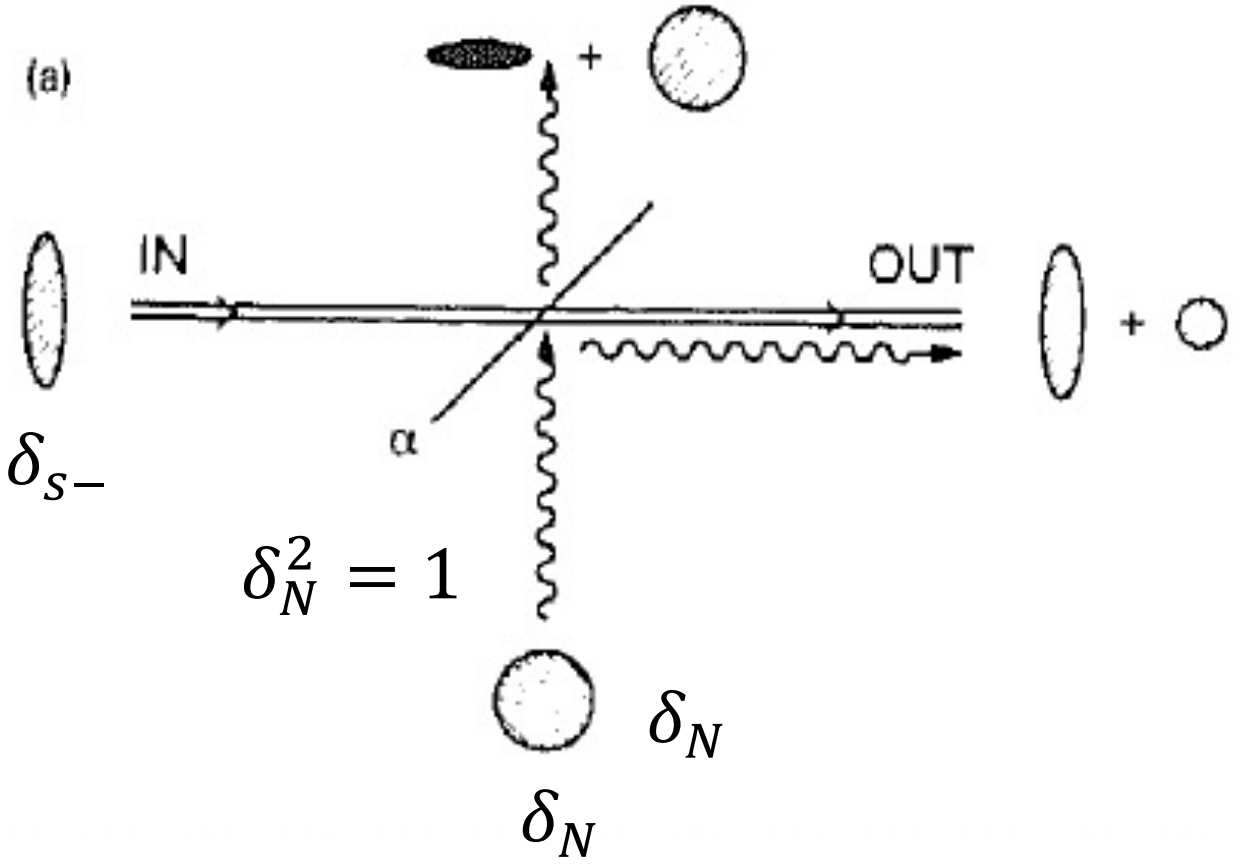

δ_{s+}

δ_{s-}

$\delta_N^2 = 1$

δ_N

δ_N

$$\frac{\delta_N + \delta_{S-}}{\sqrt{2}}$$

$$\frac{\delta_{s-}^2 + \delta_N^2}{2} < 1$$

Detector balanceado homodino. El oscilador local A_L es muy grande comparado con la señal δ_Q el espejo semitransparente es perfecto: $r = t = {}^{1}/_{\sqrt{2}}$

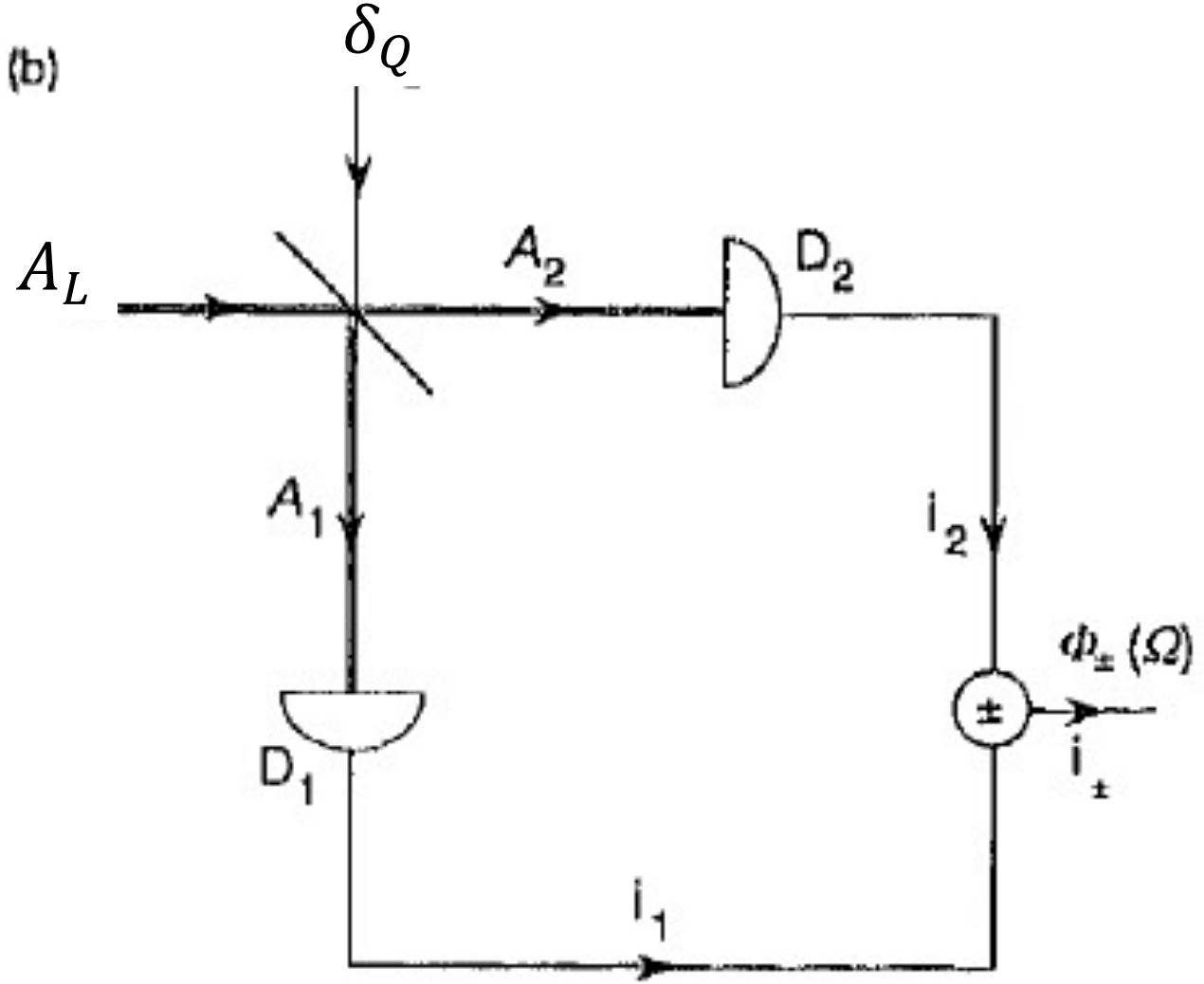

fotocorrientes en los dos detectores con ruido de disparo [δ_{SN}], técnico [δ_T], y cuántico [δ_Q]:

$$i_1 \sim \left|\frac{A_L + \delta_{SN} + \delta_T + \delta_Q}{\sqrt{2}}\right|^2 \cong \frac{{A_L}^2 + 2A_L\delta_{SN} + 2A_L\,\delta_T + 2A_L\delta_Q}{2}$$

$$i_2 \sim \left|\frac{A_L + \delta_{SN} + \delta_T - \delta_Q}{\sqrt{2}}\right|^2 \cong \frac{{A_L}^2 + 2A_L\delta_{SN} + 2A_L\,\delta_T - 2A_L\delta_Q}{2}$$

ruido en la suma y resta de las fotocorrientes; el ruido técnico es común a los dos canales, es igual y se resta. Despreciando términos de segundo orden el el ruido:

$$\delta i_+ = 2\left(A_L\delta_{SN} + A_L\,\delta_T + A_L\delta_Q\right)$$

$$\delta i_- = 2\left(A_L\delta_{SN} + A_L\delta_Q\right)$$

La razón de señal a ruido en un interferómetro de Michelson (LIGO) sin tomar en cuenta el ruido técnico

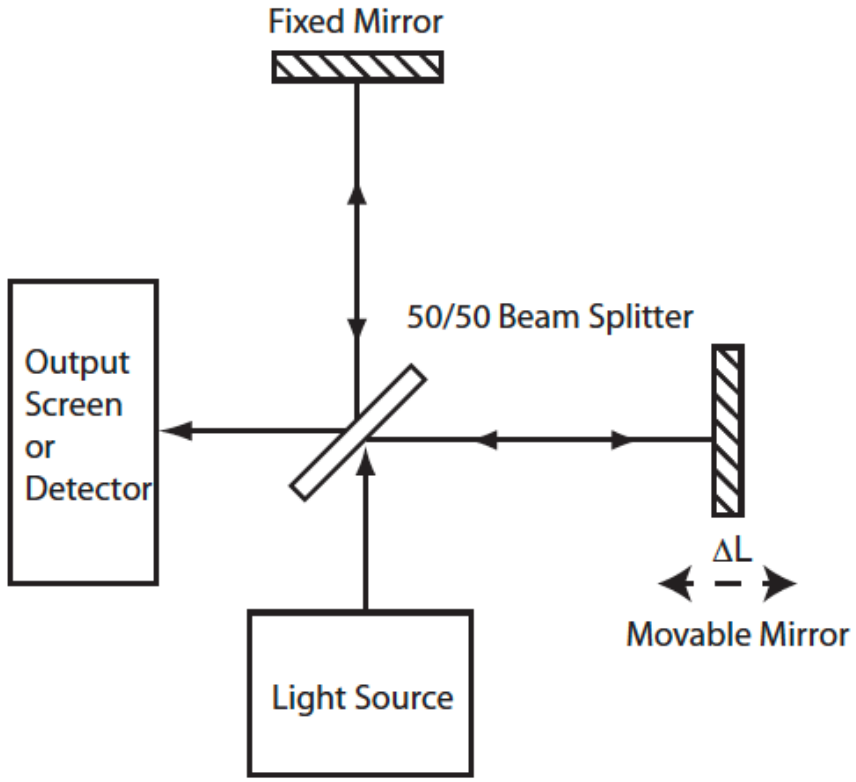

$$I_{out} = I_0 \left(A + B \cos^2 \frac{\delta}{2} \right)$$

$$\delta = 2\pi \frac{2\Delta L}{\lambda}$$

$$
\begin{aligned}
S &= I_0 \left(\cos^2 \frac{\delta - \epsilon}{2} - \cos^2 \frac{\delta + \epsilon}{2} \right) \\
S &= I_0 \left(\left(\cos^2 \frac{\delta}{2} + \epsilon \sin \frac{\delta}{2} \cos \frac{\delta}{2} \right) - \left(\cos^2 \frac{\delta}{2} - \epsilon \sin \frac{\delta}{2} \cos \frac{\delta}{2} \right) \right) \\
S &= 2 I_0 \epsilon \sin \frac{\delta}{2} \cos \frac{\delta}{2}
\end{aligned}
$$

$$
\begin{aligned}
\frac{\partial S}{\partial \delta} &= I_0 \epsilon (\cos^2 \delta/2 - \sin^2 \delta/2) \\
\frac{\partial S}{\partial \delta} &= 0 \\
\delta/2 &= \pi/4
\end{aligned}
$$

Donde la respuesta es lineal, a media banda de interferencia

$$\frac{S}{N} = \frac{I_0 \cos^2 \frac{\delta+\epsilon}{2} - I_0 \cos^2 \frac{\delta-\epsilon}{2}}{\sqrt{I_0 \cos^2 \frac{\delta+\epsilon}{2} + I_0 \cos^2 \frac{\delta-\epsilon}{2}}}$$

$$N \approx \sqrt{2I_0 \cos^2 \tfrac{\delta}{2}} = \sqrt{2I_0} \cos \tfrac{\delta}{2}.$$

$$\begin{aligned} \frac{S}{N} &= \frac{2I_0 \epsilon \sin \frac{\delta}{2} \cos \frac{\delta}{2}}{\sqrt{2I_0} \cos \frac{\delta}{2}} \\ &= \sqrt{2I_0} \epsilon \sin \frac{\delta}{2} \end{aligned}$$

$$\frac{\partial}{\partial \delta}\left(\frac{S}{N}\right) = \frac{\sqrt{2I_0}}{2} \epsilon \cos \frac{\delta}{2}$$

$$\delta/2 = \pi/2,$$

En la parte obscura de la banda de interferencia

Addition of squeezing in an interferometer and at LIGO

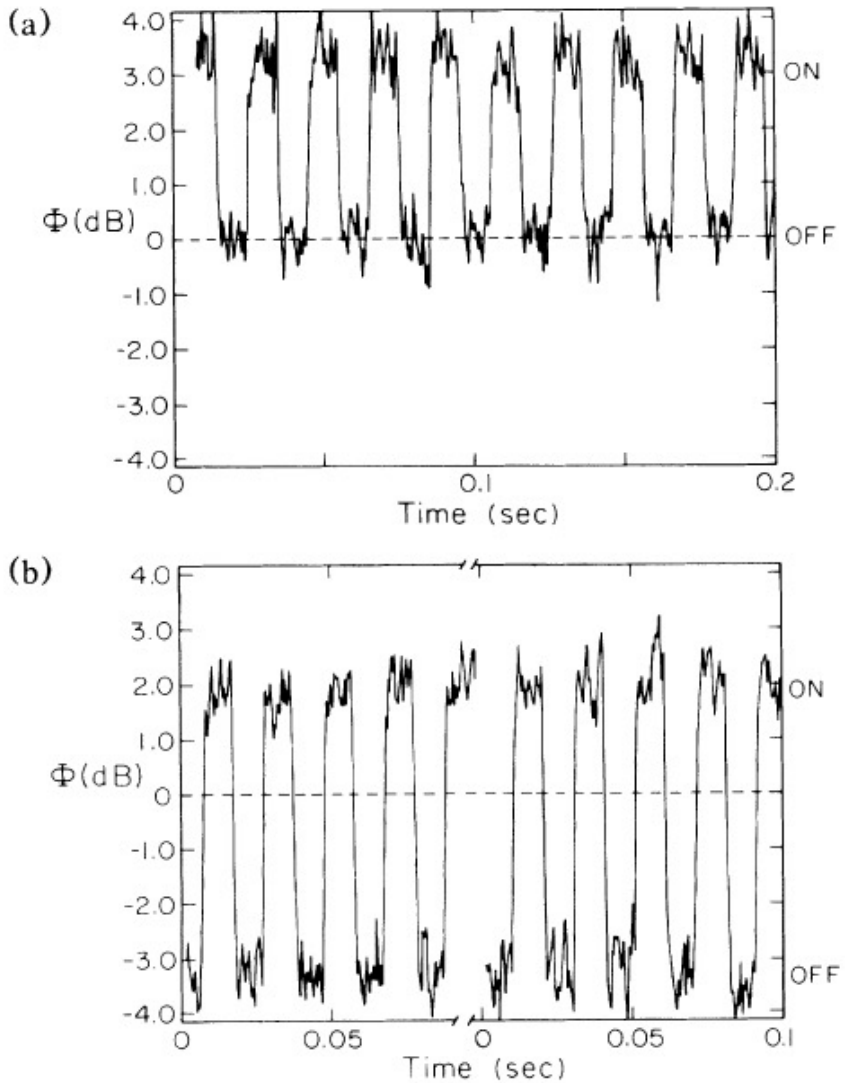

FIG. 2. Level of fluctuations Φ of the difference photocurrent i vs time for fixed analysis frequency $\nu/2\pi = 1.6$ MHz, analysis bandwidth $B = 100$ kHz, and two video filters of time

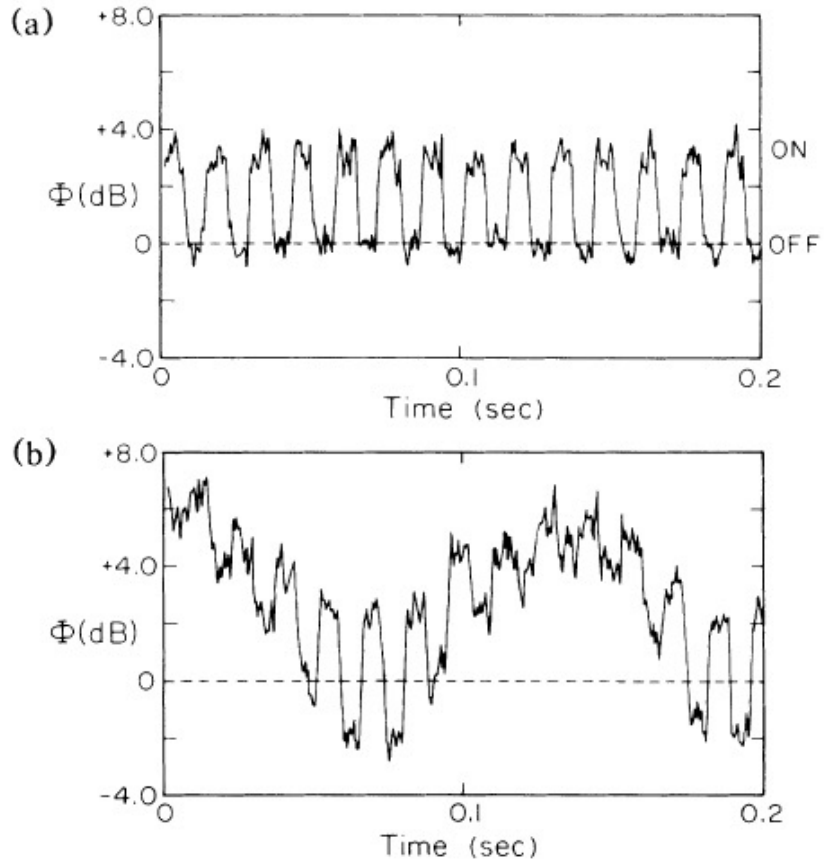

FIG. 3. Level of fluctuations Φ of the photocurrent i vs time. Parameters are similar to those in Fig. 2 with the exception that the phase angle θ is slowly swept with a linear ramp. (a) Vacuum-state input for the field $\hat{E}_s$; (b) Squeezed-state input $\hat{E}_s$. The variation of θ produces alternately a degradation and an improvement in signal to noise as first the increased $(S > 0)$ and then the decreased $(S < 0)$ fluctuations of the squeezed state are combined with the coherent field $\hat{E}_1$.

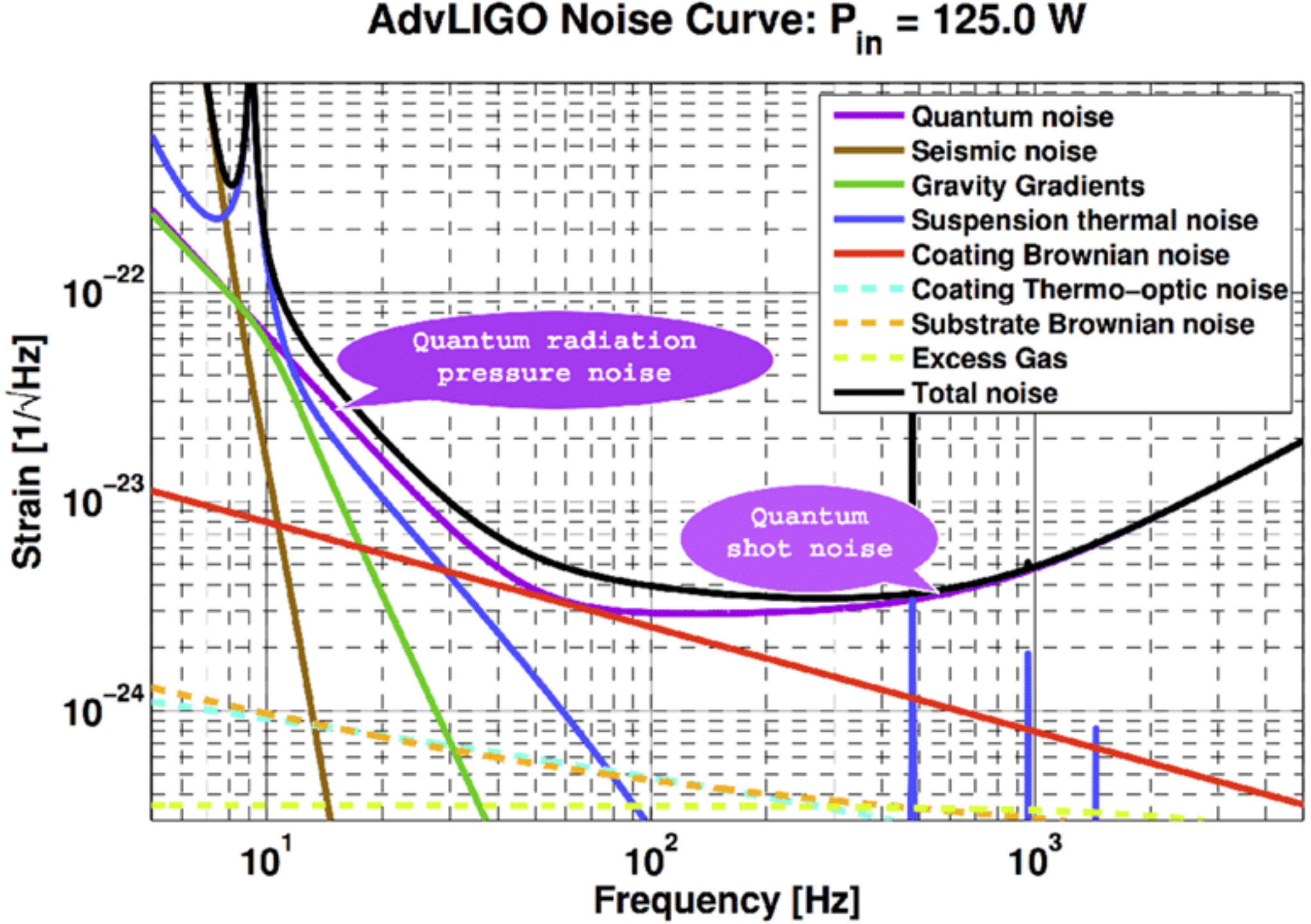
AdvLIGO Noise Curve: P_in = 125.0 W
Quantum noise
Seismic noise
Gravity Gradients
Suspension thermal noise
Coating Brownian noise
Coating Thermo–optic noise
Substrate Brownian noise
Excess Gas
Total noise
Quantum radiation pressure noise
Quantum shot noise
Strain [1/√Hz]
10^-22
10^-23
10^-24
10^1
10^2
10^3
Frequency [Hz]

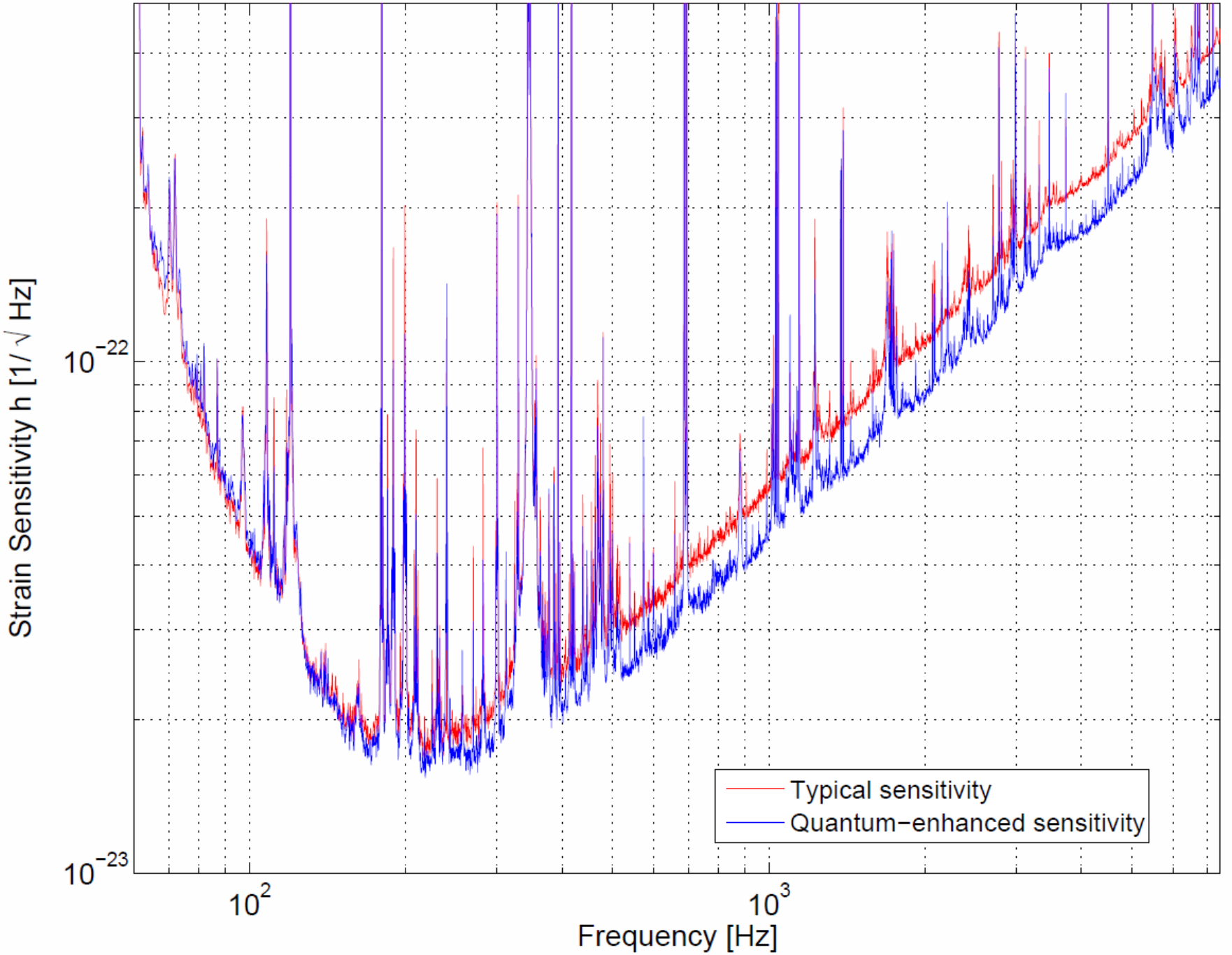
Strain Sensitivity h [1/√ Hz]
10^−22
10^−23
10^2
10^3
Frequency [Hz]
Typical sensitivity
Quantum−enhanced sensitivity

Referencias:

1. Philip R. Bevington, and D. Keith Robinson, Data Reduction an Error Analysis for the Physical Sciences.
2. Particle Data Group, https://pdg.lbl.gov/2023/reviews/mathematical_tools.html
Sección 39 de probabilidad y sección 40 de estadística.
3. Buró Internacional de Pesas y Medidas https://www.bipm.org/en/
MIT Open Courses delivered by Gilbert Strang
https://ocw.mit.edu/courses/mathematics/18-06-linear-algebra-spring-2010/video-lectures/
https://ocw.mit.edu/courses/mathematics/18-06-linear-algebra-spring-2010/syllabus/

G. T. Foster, L. A. Orozco, H. J. Carmichael, and H. M. Castro-Beltran " Quantum State Reduction and Conditional Time Evolution of Wave-Particle Correlations in Cavity QED," Phys. Rev. Lett. **85**, 3149 (2000).

H. J. Carmichael, G. T. Foster, L. A. Orozco, J. E. Reiner, and P. R. Rice " Intensity-Field Correlations of Non-Classical Light ". Progress in Optics, Vol. 46, 355-403, Edited by E. Wolf Elsevier, Amsterdam (2004).

H. J. Kimble, “Quantum Fluctuations in Quantum Optics – Squezing and Related Phenomena. Les Houches, Session LIII, (1990). J. Dalibard, J. M. Raimond, and J. Zimm-Justin editors. Systemes Fondamentaux et Optique Quantique/ Fundamental Systems inb Quntum Optics, Elsevier, Amsterdam.

Gracias